INVESTIGATION OF ν_μNe AND $\bar{\nu}_\mu$Ne INTERACTIONS AT 10.5 GeV/c*†

W. M. Yeager, W. D. Walker, W. J. Robertson, J. S. Loos, J. W. Lamsa, A. T. Goshaw, L. R. Fortney, J. R. Elliott‡

Physics Department, Duke University, Durham, North Carolina 27706

C. R. Sun and S. Dhar§

Physics Department, State University of New York, Albany, New York 12222

* Work supported by the U. S. Energy Research and Development Agency, Contract No. E-(40-1)-3065.

† Work based in part on the dissertation submitted by W. M. Yeager to the Duke University Graduate School in partial fulfillment of the requirements for the Ph. D. degree.

‡ Present address: Physics Department, University of Illinois, Urbana, Illinois 61801.

§ Present address: Physics Department, University of Massachusetts, Amherst, Massachusetts 01002.

Ly Doc Zachay 5/15/77

ABSTRACT

Detailed studies of π^+Ne and π^-Ne interactions at 10.5 GeV/c have been carried out. Multiplicities, correlations, and inclusive momentum and rapidity spectra for π^+, π^-, π^0, and p are reported. Average multiplicities for K^0 and Λ^0 production are also determined. Comparisons are made to results from πp interactions. Relative to πp collisions, pion production is enhanced in the target fragmentation region but not in the central or projectile fragmentation regions. Many of the pion production properties can be understood in terms of a simple kinematical model in which the effective target mass is greater than a nucleon mass. A surprising number of energetic protons are observed (laboratory momentum $\gtrsim$1.3 GeV/c). For shower-track multiplicities ~8, the produced nucleons are found to carry away an average of 40% of the incident momentum, indicating the possible existence of previously unrecognized mechanisms for the efficient momentum transfer to nucleons in particle-nucleus collisions.

I. INTRODUCTION

During the past several years there has been a growing interest in hadron-nucleus collisions in the multi-GeV energy region.[1] Much of this interest stems from the possibility that a nuclear target, having a thickness of several fm, might serve as an analyzer for the space-time development of hadronic states passing through nuclear matter. The possibility also exists that the experimental study of these collisions might yield new information, not readily accessible in hadron-nucleon interactions, concerning the internal structure of hadrons.

A great deal of experimental information on hadron-nucleus collisions has been gathered over a period of 25 or more years. In the early years of this period, most of this work was accomplished using cosmic rays incident on photographic emulsions.[1] Recent experimental work, using proton and pion beams from accelerators, has been done by means of emulsion,[2-7] bubble chamber,[8-12] and electronic techniques.[13-15] In these experiments, particles over a wide range of incident energy have been used to strike targets having atomic numbers from A = 1 to A = 238. Several important features of these collisions have been established, among which are: (1) R_A (defined as the ratio of mean multiplicities for p-A or π-A interactions to that for p-p or π-p interactions) is a small number that depends only weakly on the incident energy. (2) R_A grows very slowly with A. (3) hadron-nucleus interactions exhibit an approximate scaling of the Koba-Nielsen-Olesen type,[16,17] (4) the mean shower

multiplicity grows nearly linearly with the multiplicity of identified protons, (5) several energetic nucleons are sometimes ejected from the collision, and (6) particle production, relative to that from hadron-nucleon interactions, is approximately unchanged in the projectile fragmentation region but is significantly enhanced in the target fragmentation region.

A variety of theoretical and phenomenological ideas have been advanced in attempts to understand hadron-nucleus collisions. One very simple scheme supposes that particles are produced immediately at points of collision and that these particles cascade independently as they proceed through the nucleus;[18,19] however, this model is completely refuted by the experimental results on multiplicities. The parameterizations proposed by the energy-flux-cascade model[20] and the coherent-tube model[21,22] both enjoy some success in explaining the existing data, although the philosophies of these two models are quite different. The need to include the effects of special relativity in these collisions has long been recognized.[20,23-25] In particular, one expects that a hadronic state produced at the first collision should behave approximately as a single particle as it proceeds through the remainder of the nucleus, provided that it has a mean decay length, $\gamma c\tau$, which is large compared to the nuclear diameter. It is interesting that this idea alone accounts qualitatively for many of the observed experimental facts. However, a comprehensive, quantitative treatment of this complex subject does not appear likely in the near future.

In the present experiment we have made a thorough study of πNe interactions at 10.5 GeV/c using the full analyzing power of a bubble chamber. We note several advantages of the bubble chamber over other methods: a single nuclear target (Ne) may be studied; the charge and momenta of produced tracks can be determined in the magnetic field; tracks can be detected over the full 4π steradians; track density information is available; γ ray conversions and V^0 decays can be observed. Preliminary accounts of portions of this work may be found in Refs. 11 and 26. The outline of the paper is as follows: in Sect. II, a brief summary is given of the experimental techniques and analysis methods used; in Sect. III, multiplicities and correlations for π^+, π^- and p are presented; in Sect. IV, the production properties of π^+, π^-, and p are covered; in Sect. V, results on π^0, K^0, and Λ^0 production are presented; and in Sect. VI, a brief summary and conclusions are given. We trust that this comprehensive experimental investigation using one nuclear target at one bombarding energy will prove helpful in the attempt to improve the understanding of complex inelastic hadron-nucleus interactions.

II. EXPERIMENTAL TECHNIQUES AND METHODS OF ANALYSIS

A. Bubble Chamber Exposure and Pion Beam

Table I presents a summary of the data sample studied for this paper. The Stanford Linear Accelerator Center 82-inch bubble chamber was filled with a mixture of 32 molar percent Ne and 68 molar percent H_2, and exposed to π^+ and π^- beams having central momentum values of 10.46 GeV/c and 10.39 GeV/c, respectively.[28] The H_2Ne mixture had a radiation length of 125 cm.

B. Scanning and Measuring Procedures

The film was scanned for any interaction of a beam track in the upstream two-thirds of the bubble chamber. Scanned events were classified by the numbers (n_+, n_-, N_h), where N_h is the number of visually identified heavily ionizing proton tracks, n_- is the number of negatively charged tracks, and n_+ is the number of positively charged tracks which remain when all visually identified proton tracks are removed. The number of "shower tracks" is $n_s = n_+ + n_-$. Associated vertices, arising either from γ conversions or from the decay of K^0 or Λ^0 particles, were also recorded.

Five percent of the film was independently rescanned to determine scan efficiencies: 94% for events with two or more charged tracks; 90% for events with 0 or 1 charged track; 91% for associated secondary vertices. These efficiency factors have been used to correct all multiplicity

data presented in this paper. We note that nNe elastic scattering events are effectively excluded from detection because of the very small scattering angle involved.

Both np and nNe reactions occur. The expected numbers of each kind of interaction are given in Table I. From the scan information, an approximate separation of events into np and nNe categories was made. An event was classified as "hydrogenic" if $N_h < 2$ and if the net charge was consistent with a np collision; otherwise, an event was classified as "neonic." The results of these classifications are shown in Table I. We find that approximately 20% of the nNe interactions are classified as hydrogenic by this procedure. These excess hydrogenic events arise from pion interactions with a quasi-free nucleon in the Ne nucleus, where the remainder of the nucleus acts as a "*spectator*." Because we find these peripheral collisions to be similar to np collisions, appropriate fractions of the hydrogenic events have been added to the neonic events in order to provide an *inclusive* sample of "nNe interactions." Throughout this paper, we will use the terms "nNe interactions" and "np interactions" to denote the properly renormalized samples, whereas "neonic" and "hydrogenic" will be used to denote the categories defined above.

A sample of ~7500 events were measured on the semi-automatic measuring system, HIPPIE.[29] All measured events were retained for analysis even though many events had one or more tracks which failed in measurement or in reconstruction. For tracks longer than 10 cm in space, the average probability for successful measurement and recon-

struction was 0.92. This probability depended somewhat on multiplicity, ranging from 0.96 for two-pronged events to 0.87 for twelve-pronged events. Weights have been applied to the final sample to compensate for these track losses and also to assure that the multiplicity distribution from measured events corresponds to that of the scanned events. Proton tracks having very low momentum were processed rather inefficiently. Averaged over the interval $0.15 < p < 0.25$ GeV/c, approximately 45% of the scanned protons failed measurement or reconstruction. Because these losses are confined to well-defined kinematical regions, we have made no corrections for them in the distributions presented in this paper. The secondary neutral vertices (γ, K^0, Λ^0) from these events were measured separately on a conventional image plane digitizer. All tracks were spatially reconstructed using the program TVGP, which was modified to deal with the H_2Ne mixture.

Whenever possible, curvature, range, and track density information have been used to separate π^+ tracks from proton tracks. This method is quite reliable below ~0.9 GeV/c, but is not usable above ~1.3 GeV/c for the present H_2Ne mixture. Consequently, N_h often is smaller than the true number of protons and n_s often includes some protons. On a statistical basis, this ambiguity between π^+ and proton can be resolved by the isospin symmetry of the π^+Ne and π^-Ne interactions (see below), therefore, in the multiplicity and inclusive particle distributions, a separation between π^+ and p can be made. The presence of K^+ tracks has been ignored in this study. This is justified because the ratio of K^+/π^+ is only approximately 1.5%, as determined by our study of K^0 production (see Section V).

C. Isospin Symmetry of π^-Ne and π^+Ne Interactions

We have made use of the isospin symmetry of π^+Ne and π^-Ne systems in order to untangle the ambiguities between π^+ and proton distributions. Under reversal of the third component of isospin, we have $\pi^+ \leftrightarrow \pi^-$, $p \leftrightarrow n$, and Ne $\leftrightarrow$ Ne (Ne is an I=0 nucleus). For example, the following relations (and similar relations) must hold:

$$\langle n_{\pi^+} \rangle_{\pi^+\mathrm{Ne}} = \langle n_{\pi^-} \rangle_{\pi^-\mathrm{Ne}}$$

$$\langle N_p \rangle_{\pi^+\mathrm{Ne}} = \langle N_n \rangle_{\pi^-\mathrm{Ne}}$$

where, e.g., $\langle N_p \rangle_{\pi^+\mathrm{Ne}}$ is the average number of protons produced in π^+Ne collisions. More generally, we have the relation

$$f(n_{\pi^+}, n_{\pi^-}, n_{\pi^0}, N_p, N_n)_{\pi^+\mathrm{Ne}} = f(n_{\pi^-}, n_{\pi^+}, n_{\pi^0}, N_n, N_p)_{\pi^-\mathrm{Ne}}$$

where $f(\cdots)_{\pi^+\mathrm{Ne}}$ represents any function of the produced particles for π^+Ne collisions. Further details of our use of isospin symmetry are given with the presentation of the data in Sections III-VI.

D. Weights and Corrections for γ, K^0, and Λ^0 Particles

Each observed γ conversion (or decay of K^0 or Λ^0) was weighted by a factor $w = P^{-1}$, where P is the probability for observation:

$$P = \exp(-L_{min}/\lambda) - \exp(-L_{max}/\lambda) .$$

In this expression λ is the conversion (or decay) length, and L_{min} (L_{max}) is the minimum (maximum) allowable neutral track length. In

order to avoid confusion with tracks from the primary interaction, L_{min} was chosen to be 2 cm. For γ conversions, L_{max} was chosen to be the smaller of 120 cm or D_{max}, where D_{max} is the maximum potential length to the edge of the fiducial volume. For K_s^0 or Λ^0 decays, L_{max} was chosen to be the smaller of 2.5 λ or D_{max}. The average probability of an e^+e^- conversion within the fiducial volume is approximately 0.20.

Approximately 8% of the e^+e^- pairs were rejected after measurement on the basis of pointing tests or bremsstrahlung origin tests.[30] Approximately 6% of the K^0 and Λ^0 particles also failed a pointing test. Corresponding corrections have been made to the weights of the surviving pairs or decays.

Corrections for radiative losses for the e^+e^- pairs were also made. The typical correction is 3-5% in the energy of the pairs.

III. CHARGED PARTICLE MULTIPLICITIES AND CORRELATIONS

A. Averaged Multiplicities of Charged Particles

The averaged particle multiplicities are given in Table II. In obtaining these averages, it has been assumed that the charged particles are π^+, π^-, *or p (that is,* $K^\pm$, $\Sigma^\pm$, $\bar{p}$, *etc, have been ignored). Applying the requirements of charge symmetry, we then find the following relations:*

$$\langle n_{\pi^+} \rangle_{\pi^+ Ne} = \langle n_{\pi^-} \rangle_{\pi^+ Ne} = \langle n_- \rangle_{\pi^+ Ne} ,$$

and

$$\langle N_p \rangle_{\pi^+ Ne} = \langle N_h \rangle_{\pi^+ Ne} + \langle n_+ \rangle_{\pi^+ Ne} - \langle n_- \rangle_{\pi^+ Ne} .$$

Thus we are able to find $\langle n_{\pi^-} \rangle$, $\langle n_{\pi^+} \rangle$, and $\langle N_p \rangle$ for both reactions by measuring the quantities $\langle n_- \rangle$, $\langle n_+ \rangle$, and $\langle N_h \rangle$ for both reactions.

In Table III, we summarize the values for $\langle n_\pi \rangle = \langle n_{\pi^+} \rangle + \langle n_{\pi^-} \rangle$, the average number of pions produced in inelastic π^+Ne interactions, and the values of R, defined as

$$R = \frac{\langle n_\pi \rangle_{\pi Ne}}{\langle n_\pi \rangle_{\pi p}} .$$

The values of R are found to be near unity. Averaging over π^+*Ne and* π^-*Ne, we have* $R_{Ne} = 1.08 \pm 0.03$.

Much attention has been given to the ratio R *in hadron-nucleus interactions. The results of many experiments have shown that* R *is small, grows very slowly with increasing atomic number, and is nearly*

independent of bombarding energy for fixed atomic number.[2-6,11-14] These facts clearly rule out models in which all produced particles are allowed to cascade independently in the nucleus.[13-19] However, the behavior of R can be accomodated by several quite different models in which the evolution time of the scattered projectile fragments is comparable to or longer than the time between successive collisions inside the nucleus. In the "energy flux cascade" model of Gottfried,[20] $R \simeq 1 + a(\langle \nu \rangle - 1)$, where ν is the number of collisions of the projectile system in passing through the nucleus, and where the usual value of the parameter a is approximately 1/3. For πNe interactions, we have $\langle \nu \rangle_{Ne} = A\, \sigma_{inel}(\pi p)/\sigma_{inel}(\pi Ne) \simeq 1.6$. The present result, $R_{Ne} = 1.08$, therefore implies that $a \simeq 0.12$, which is somewhat lower than the conventional value. The "coherent tube" model of Berlad, Dar, and Eilam[21] predicts $R \simeq \langle \nu^{1/4} \rangle$ where the evaluation of $\langle \nu^{1/4} \rangle$ depends to some extent on the assumed nuclear shape. Taking the nucleus to be a uniform sphere, we find that $R_{Ne} = \langle \nu^{1/4} \rangle_{Ne} \simeq 1.1$, in good agreement with the data, provided that a value of $\langle \nu \rangle_{Ne} = 1.6$ is used.[32]

We note that the models discussed in the previous paragraph are designed for high-energy collisions, and therefore may not be wholly applicable at energies as low as 10.5 GeV. At this relatively low energy, a complete description of hadron-nucleus collisions would have to consider the effect of absorption and would have to account for some independent cascading of the wide-angle particles.

B. Multiplicity Distributions Corrected for Ambiguities between p and π^+

The observed scanned events for $\pi^{\pm}$Ne interactions provide multiplicity distributions in the variables n_+, n_-, and N_h. These distributions are denoted by $g^{\pm}(n_+, n_-, N_h)$. We now discuss the procedure used to determine the corresponding distributions, $h^{\pm}(n_{\pi^+}, n_{\pi^-}, N_p)$. These latter distributions will be called the "corrected" distributions.

In Table IV we present the experimental distributions, $G^{\pm}(n_+, n_-)$, where

$$G^{\pm}(n_+, n_-) \equiv \sum_{N_h} g^{\pm}(n_+, n_-, N_h)$$

That is, $G^{\pm}(n_+, n_-)$ is just the distribution of positively and negatively charged shower tracks, summed over N_h. If all produced protons had been classified among the N_h heavily ionizing particles, then we would expect to find $n_+ = n_{\pi^+}$ and $n_- = n_{\pi^-}$. As a consequence of isospin requirements, we would then expect to find $G^+(n_+, n_-) = G^-(n_-, n_+)$. However, it is evident from Table IV that this relation is poorly satisfied by the raw scan data. We are therefore forced to conclude that a significant fraction of the positively charged shower tracks are protons. The number of these "fast knockout" protons in an event is $N_f = N_p - N_h$. From Table II, we find $\langle N_f \rangle = 0.78 \pm 0.13$ for π^+Ne and $\langle N_f \rangle = 0.46 \pm 0.12$ for π^-Ne.

Further evidence for the presence of protons among the shower tracks is seen in the average net charge of the shower tracks. For each

event, we define the net beam-like charge of the shower particles, Δ_s, as follows:

$$\Delta_s \equiv n_+ - n_- \qquad \text{for } \pi^+ Ne$$

$$\equiv n_- - n_+ \qquad \text{for } \pi^- Ne \ .$$

Figure 1a shows the dependence of the averaged values, $\overline{\Delta}_s$, as a function of shower multiplicity, n_s. (Recall that $n_s = n_+ + n_-$.) If there were no protons among the shower tracks, then the values of $\overline{\Delta}_s$ would be the same for $\pi^+ Ne$ and $\pi^- Ne$ events. The effect of the unidentified proton tracks is readily apparent; the average number of such proton tracks per event grows from ~ 0 for $n_s = 1$ to ~ 1 for $n_s = 8$.

In order to determine the corrected distributions, $h^{\pm}(n_{\pi^+}, n_{\pi^-}, N_p)$, it is necessary to redistribute the n_+ tracks from the observed events. That is, the observed events in $g^{\pm}(n_+, n_-, N_h)$ must contribute to the events in $h^{\pm}(n_+ - m, n_-, N_h + m)$, where $m = 0, 1, 2 \cdots$. We have found from the data that this redistribution appears to be independent of N_h. Thus we define

$$H^{\pm}(n_{\pi^+}, n_{\pi^-}) \equiv \sum_{N_p} h^{\pm}(n_{\pi^+}, n_{\pi^-}, N_p) \ .$$

That is, $H^{\pm}(n_{\pi^+}, n_{\pi^-})$ is the multiplicity distribution, summed over N_p, for producing n_{π^+} positive pions and n_{π^-} negative pions. As discussed in detail in Appendix A, a suitable parameterization was devised to determine a least-squares fit for the $H^{\pm}(n_{\pi^+}, n_{\pi^-})$ distributions from

the $G^{\pm}(n_+, n_-)$ distributions. The fit was subjected bin-by-bin to the isotopic spin constraint,

$$H^{+}(n_{\pi^+}, n_{\pi^-}) = H^{-}(n_{\pi^-}, n_{\pi^+}) \quad ,$$

for $0 \leq n_{\pi^+} \leq 7$ and $0 \leq n_{\pi^-} \leq 7$. The fit was further constrained such that the final averaged pion multiplicities, $\langle n_{\pi^+} \rangle$ + $\langle n_{\pi^-} \rangle$, were consistent with the results given in Table II. In addition, the overall net charge of the fitted pion multiplicities were required to be consistent between π^+Ne and π^-Ne interactions.

The fitted $H^{\pm}(n_{\pi^+}, n_{\pi^-})$ distributions, which are hereafter called the "corrected" pion multiplicity distributions, are displayed in Table V. The complete three dimensional distributions, $h^{\pm}(n_{\pi^+}, n_{\pi^-}, N_p)$, are somewhat voluminous and are not presented in this paper. However, in Table VI we do show the collapsed distributions in the variables N_p and n_π, where $n_\pi = n_{\pi^+} + n_{\pi^-}$. Results based on these corrected distributions are presented in Section III. C below.

The excellent agreement between $H^{+}(n_{\pi^+}, n_{\pi^-})$ and $H^{-}(n_{\pi^-}, n_{\pi^+})$ in Table V attests to the adequacy of the correction procedure. A further check of this method is shown in Fig. 1b, which is a plot of the average net charge of the pion tracks versus n_π. In this figure, we define Δ_π by:

$$\Delta_\pi \equiv n_{\pi^+} - n_{\pi^-} \qquad \text{for } \pi^+\text{Ne}$$

$$\equiv n_{\pi^-} - n_{\pi^+} \qquad \text{for } \pi^-\text{Ne}$$

Excellent agreement is again found between the corrected π^+Ne and π^-Ne results. We conclude that the present correction procedure is quite reliable. It is perhaps worth stressing again that the success of this procedure has depended critically on the stringent requirements of charge symmetry.

C. Results from the Corrected Multiplicity Distributions

The multiplicity distributions in n_s, the number of charged shower particles per event, and in n_π, the number of charged pions per event, are given in Table VII. These distributions are readily obtained from Tables IV and V. The dispersion parameter for the charged pion multiplicity is $\left(\langle n_\pi^2\rangle - \langle n_\pi\rangle^2\right)^{1/2} = 1.99 \pm 0.03$. In Fig. 2, the n_π distribution (averaged over the π^+Ne and π^-Ne results) is displayed in the KNO scaling form[16,17] and is compared to π^-Ne results at 200 GeV/c[11] and to π^+p and π^-p data interpolated to 10.5 GeV/c.[5,6,9,11] The scaled πNe distributions are in very good agreement with each other, and are consistent with KNO scaling. Agreement with KNO scaling for particle-nucleus interactions has been found previously. The πNe and πp distributions are also similar, although the πNe shape is clearly broader. This broadening could be caused by multiple collision processes in the nucleus, but it also could result from kinematic limitations at the relatively low energy of the present experiment.

In Fig. 3 we display the distribution in Δ_π, the net charge of the pion tracks. The π^+Ne and π^-Ne data have been averaged in this plot. Multiple

collisions involving charge exchange can cause the net charge of the pions to migrate to a final value considerably different from the charge of the incident beam particle. However, this does not appear to occur very often since only 12% of the events have $|\Delta_\pi - 1| > 1$. The hand-drawn dashed lines show an exponential decrease proportional to $\exp(-2.1|\Delta_\pi - 1|)$ for $\Delta_\pi > 0$ and proportional to $\exp(-1.7|\Delta_\pi - 1|)$ for $\Delta_\pi < 0$.

The multiplicity distributions in N_h, the number of identified heavily ionizing protons, and in N_p, the corrected number of protons, are given in Table VIII. The N_p distributions are also plotted in Fig. 4. The N_p distribution for π^+Ne is somewhat broader than that for π^-Ne, as required by the values for $\langle N_p \rangle$ given in Table II. As N_p increases, both spectra fall in a smooth way somewhat faster than exponentially. The numbers of protons produced per event reflects the disruption of the struck nucleus, and in an average way, should measure the number of elementary collisions of the beam or beam fragments with the nucleons in the nucleus. It is interesting to observe that in $\sim 1\%$ of the events, nine or more protons emerge (all having laboratory momenta above ~ 0.15 GeV/c); such events are likely to result from a combination of several (~ 3) elementary collisions of the beam fragments in conjunction with several secondary collisions of particles produced at wide angles. Note that isospin symmetry implies that the N_p distribution for π^-Ne is identical to the neutron distribution for π^+Ne, and vice-versa. Therefore the dashed

(solid) histogram in Fig. 4 can also be viewed as the neutron multiplicity distribution for π^+ Ne (π^- Ne) interactions.

The correlations between n_π and N_p are of considerable interest since they are sensitive to the details of the intranuclear cascade processes.[33] In Fig. 5a we present the scaled charged pion multiplicity versus N_p. For $N_p < 5$, the pion multiplicity is found to grow roughly as $\langle n_\pi(N_p) \rangle / \langle n_\pi \rangle \simeq 0.8 + 0.1\ N_p$ (dashed line). Similar correlations have been observed in proton-nucleus studies[3-6,12] and in π-nucleus studies.[11,13] This linear growth is likely to be caused by an increase in the average number of interactions within the nucleus. Beyond $N_p \sim 5$, there appears to be a saturation in $\langle n_\pi(N_p) \rangle$ that is perhaps caused by the finite size of the Ne nucleus.

In Fig. 5b we show, as a function of N_p, the ratio of the dispersion parameter divided by average number of charged pions. A linear relationship is found: $D(N_p)/\langle n_\pi(N_p) \rangle \simeq 0.62 - 0.03\ N_p$. This means that, as a function of N_p, the dispersion of the multiplicity grows more slowly than the average multiplicity. This effect, at least in part, may be caused by kinematic restrictions at 10.5 GeV/c since it is difficult to produce more than ~ 10 pions at this relatively low energy, especially in central (high N_p) collisions. It would be of interest to examine the behavior of this ratio at higher energies. We also note that the present results imply that the same KNO scaling function cannot describe exactly the charged pion multiplicity spectra for all values of N_p (at 10.5 GeV/c).

In Fig. 6, the average number of protons per event, $\langle N_p(n_\pi) \rangle$, is plotted versus n_π. Again, a nearly linear growth is found. The results of Figs. 5 and 6, taken together, imply that events with large values of n_π tend to have large values of N_p, and vice-versa. In other words, as the violence of a particle-nucleus collision is increased, a simultaneous growth of n_π and N_p is found.

Andersson[1] has suggested that it should be interesting to examine the correlations between n_π and the number of lightly-ionizing (fast knock-out) protons, N_f, because N_f (rather than N_p or N_h) might provide the best measure of the number of elementary collisions of the projectile or its fragments with the nucleons in the nucleus. Although a fast knock-out proton cannot be distinguished from a positive pion on a track-by-track basis, the correction procedure discussed above does provide a statistical method for obtaining charged pion multiplicity distributions corresponding to various values of N_f. The reader is cautioned that the parameter N_f defined in this way overestimates the number of energetic protons ($p > 1.0$ GeV/c) by a factor of approximately 1.5 because unrecognized low energy protons are also included. In Fig. 7a and Fig. 7b, respectively, we show the averaged multiplicity, $\langle n_\pi(N_f) \rangle$, and the ratio, $D(N_f)/\langle n_\pi(N_f) \rangle$, as functions of N_f. The π^+Ne and π^-Ne results have been averaged in these plots. The behavior of these quantities as functions of N_f is quite similar to their behavior as functions of N_p (see Fig. 5). Apparently both N_f and N_p are reasonable measures of the number of elementary collisions.

IV. PRODUCTION OF CHARGED PIONS AND PROTONS

A. Introduction

In this section we present data on charged particle production in πNe interactions and compare them to the results of πp interactions. These data should provide insight into the characteristics of hadron shower development within a nucleus and should be useful for testing models of hadron-nucleus collisions.

For convenience of expression, we define "favored" and unfavored" pions to be produced as follows:

$$\pi^{\pm} Ne \rightarrow \pi^{\pm} X \quad \text{(favored)} \ ,$$

and

$$\pi^{\pm} Ne \rightarrow \pi^{\mp} X \quad \text{(unfavored)} \ .$$

That is, the favored (unfavored) pions have the same (opposite) charge as the incident particle. These terms will also be used to reference πp interactions.

We use the symbols p_L, p_T, E, and y to represent, respectively, the longitudinal momentum, transverse momentum, energy, and rapidity variables in the laboratory system. Symbols with an asterisk (e.g., y^*) are used to represent variables in the center of mass system of the incoming pion and a single nucleon.

Extensive use is again made of the isospin symmetry between π^+Ne and π^-Ne. For example, the longitudinal momentum distributions of favored (or unfavored) pions for π^+Ne and π^-Ne should be equal:

$$\frac{d\sigma}{dp_L}(\pi^+)_{\pi^+Ne} = \frac{d\sigma}{dp_L}(\pi^-)_{\pi^-Ne}$$

Thus the inclusive π^+ distributions can be found for both reactions by measuring both of the inclusive π^- distributions. [Note that we have assumed that all negatively charged tracks are pions.] We also can determine the inclusive momentum spectrum of the unidentified lightly ionizing protons (fast knockout protons) by subtracting the spectrum for negatively charged shower tracks from that for positively charged shower tracks. For example:

$$\frac{d\sigma}{dp_L}(p_f)_{\pi^+Ne} = \frac{d\sigma}{dp_L}(\pi^+)_{\pi^+Ne} - \frac{d\sigma}{dp_L}(\pi^-)_{\pi^-Ne} ,$$

where p_f refers to an unidentified proton and π^+ (π^-) refers to a positively (negatively) charged shower track. This subtraction technique is valid for any variable or combination of variables that do not depend upon the masses of the particles (e.g., valid for momenta but not for rapidity).

B. Charged Pion Distributions

We find that the most significant differences between πNe and πp single pion distributions occur in the target fragmentation region. This is shown in Fig. 8, where the invariant structure function for charged pions, integrated over p_T^2, is plotted versus p_{L^*}. In order to facilitate the comparison between πNe interactions (solid histograms) and πp interactions

(dashed histograms), the invariant structure functions have been divided by the appropriate inelastic cross sections.[34] In the target fragmentation region ($p_L \lesssim 1$ GeV/c), there is a clear excess of the πNe distribution over the πp distribution. For both the favored and unfavored pions, the ratio of production from πNe to that from πp is seen to grow from ~1 to ~3 as p_L is decreased from ~1 GeV/c to zero. This large relative increase in pion production in the target fragmentation region appears to be a fundamental feature of hadron-nucleus collisions. We also note that a portion of this excess π^- production is expected on the basis of charge conservation because the process $\pi^+ n \to \pi^- X$ (which occurs inside the Ne nucleus) is favored relative to the process $\pi^+ p \to \pi^- X$.

The inclusive single pion rapidity spectra from πNe and πp interactions are shown and compared in Fig. 9. For both the favored and unfavored pion distribution, we find: (1) for $y^* < 0$, pion production from πNe is two or three times as large as that from πp; (2) the πNe and πp spectra converge near $y^* = 0$; and (3) the πNe and πp distributions remain nearly equal for the entire forward hemisphere, $y^* > 0$. These trends are further illustrated by the ratios of the πNe to πp distributions in Fig. 10. In the projectile fragmentation region ($y \sim 4$), this ratio is approximately 0.8 for the favored pions, and is in mild disagreement with results at higher energies where a ratio near unity is found.[6,7,13,15] It is possible that the absorption of projectile fragments is greater at low energies than at high energies because there is more time for the projectile system to develop before leaving the nucleus.

The similarity seen in the region $y^* > 0$ implies that the fragments of the projectile system must act nearly as a single particle as the system proceeds through the nucleus. That is, the evolution time of the projectile system must be long relative to its transit time across the nucleus, and repeated collisions within the nucleus have little effect on the final projectile fragments. On the other hand, the target fragments are significantly enhanced by the multiple collisions in the nucleus, and it is this portion of the rapidity spectrum that contributes to the rise in multiplicity from a nucleus relative to a nucleon.

It is of interest to ask whether there is a leading particle effect for the favored pions produced in πNe collisions. As is seen from Table 2, there are 0.71 ± 0.03 more favored pions than unfavored pions per event. The kinematic regions into which these excess favored pions are produced are evident in Table IX, where we give the average number of π^- per event observed in various intervals of y and N_h. Large excesses of favored pions are found in the central and projectile rapidity regions when $N_h \lesssim 1$, but only small excesses are seen elsewhere. Thus we can conclude that the leading particle effect is present for the peripheral πNe interactions ($N_h \lesssim 1$) but not for the non-peripheral interactions ($N_h > 2$).

Many of the properties of hadron-nucleus collisions can be related to those from hadron-nucleon collisions by assuming that in a nucleus the incident hadron can collide conjointly with more than one nucleon. The effective mass of the target, and therefore the available center-of-

mass energy is increased in a nuclear target relative to a nucleon target. These ideas have been considered for some time.[24,35] The "coherent tube" model[21,22] is a recent extension of these ideas. In order to make definite predictions for the ^{4}Ne rapidity data, we assume that the incident particle collides with ν nucleons in the nucleus in such a way that the effective target mass is νM, where M is the nucleon mass. The produced spectrum is then assumed to be equal to that for a single nucleon collision, but at an elevated energy given by

$$s = m^2 + (\nu M)^2 + 2\nu M(p^2 + m^2)^{1/2}$$
$$\simeq 2\nu M p$$

where p is the laboratory momentum of the incident pion and m is the pion mass (which may be ignored at the present energies). The rapidity distribution in y^* must then be boosted to the laboratory system for each value of ν, as follows:

$$y_\nu = y^* + \xi_\nu \quad ,$$

where

$$\xi_\nu = \frac{1}{2} \ln \frac{1+\beta_\nu}{1-\beta_\nu} \simeq \frac{1}{2} \ln \left(1 + \frac{2p}{\nu M}\right) \quad .$$

β_ν is the transformation velocity between the laboratory and the center-of-mass frames. The resulting rapidity distributions can then be summed to obtain a definite prediction for a particle-nucleus collision.

We have tested such a prediction against our data for the reaction $\pi^+ Ne \rightarrow \pi^- X$. In order to average over $\pi^+ p$ and $\pi^+ n$ distributions, we have summed over $\pi^+ d$ data,[36] as follows:

$$\frac{1}{\sigma_{inel}(\pi Ne)} \frac{d\sigma}{dy} (\pi^+ Ne \rightarrow \pi^- X;\ s,\ y)$$

$$= \frac{1}{\sigma_{inel}(\pi d)} \sum_{\nu=1}^{3} \alpha_\nu \frac{d\sigma}{dy} (\pi^+ d \rightarrow \pi^- X;\ s_\nu,\ y_\nu)$$

where the α_ν factors represent the fraction of πNe interactions involving ν nucleons. On the basis of a uniform Ne nucleus, we estimate $\alpha_\nu = 0.59$, 0.30, and 0.11 for $\nu = 1$, 2, and 3, respectively. (Contributions for $\nu > 3$ have been ignored.) The resulting prediction, which has no adjustable parameters,[37] is shown in Fig. 9b and is in remarkably good agreement with the data.

In Fig. 11, we plot the rapidity spectrum for the unfavored pions subdivided into three groups according to the number of heavily ionizing proton tracks: $N_h \leq 1$ (53% of the events), $2 \leq N_h \leq 4$ (38% of the events), and $5 \leq N_h \leq 10$ (9% of the events). Since N_h seems to be a rough measure of ν, we expect that these divisions should correspond approximately to $\nu = 1$, 2, and 3, respectively. The curves imposed on the data are the component distributions which make up the prediction of Fig. 9b. These curves provide a qualitatively good description of the data. As ν is increased, the component spectra are broadened (because of higher effective center-of-mass energies) and shifted to lower rapidity (because of smaller transformation velocities, β_ν). The data also show these trends. In Table X, we give the mean values of laboratory rapidity corresponding to these selections on N_h together with the calculated boost factors, β_ν.

We have also examined the rapidity distributions for the following

subdivisions: $n_s \leq 5$, $6 \leq n_s \leq 8$, and $9 \leq n_s$. Since n_s and N_h have a nearly linear correlation, we also expect these divisions to correspond approximately to $\nu = 1$, 2, and 3, respectively. The resulting rapidity distributions (not shown) exhibit trends similar to those seen in Fig. 11. The mean laboratory rapidity values for the n_s selections are given in Table X, and are in good agreement with the corresponding values for the N_h selections.

It is possible that the present agreement at 10.5 GeV/c could be a fortuitous result caused by kinematical restrictions at this energy. Definitive tests of these ideas are needed at higher energies, where at present there is some controversy over whether or not the "coherent tube" model predictions[1,22] agree with the available data.[14] Detailed comparisons are difficult at high energies both because of experimental measurement problems and because of uncertainties in the nuclear modeling and in the hadron-hadron rapidity distributions.

We turn now to the examination of distributions in transverse momentum. The principal result is that the πNe data are nearly indistinguishable from the πp data. In Fig. 12, we show the p_T^2 distributions, normalized so that the same number of tracks are plotted for the πNe and πp data. In the interval $p_T^2 < 1$ $(GeV/c)^2$, there are no significant differences between the data from the two targets; this holds both for the favored and the unfavored pions. The averages, $\langle p_T \rangle$ and $\langle p_T^2 \rangle$, are given in Table X and also show that the differences between πp and πNe are small. The values for $\langle p_T \rangle$ and $\langle p_T^2 \rangle$ are larger for the favored pions than

for the unfavored pions; this is true for both πNe and πp interactions. We also note that the averages found for πp are in good agreement with previously reported results.[38]

It might be conjectured that the transverse momentum spectrum should become broader as N_h is increased because more nucleons then tend to participate in the πNe collisions. In order to search for such an effect, we have plotted $\langle p_T \rangle$ as a function of N_h (see Fig. 13). The surprising result is that $\langle p_T \rangle$ appears to be independent of N_h, for $N_h > 1$; this is true for both the favored (solid triangles) and unfavored (solid circles) pions. For $N_h \leq 1$, differences between the favored and unfavored pions do occur; however, these $\langle p_T \rangle$ values are in good agreement with the corresponding πp values (open triangle and open circle). Also plotted in this Figure are values of $\langle p_T(N_h) \rangle$ for the most energetic (leading) π^- produced in π^-Ne events (solid diamonds) and in π^-p events (open diamond). The leading π^- particles clearly have significantly larger $\langle p_T \rangle$ values than those found by averaging over all favored pions, but again the πNe values for $\langle p_T \rangle$ are independent of N_h, and are in good agreement with the πp value.

We have also examined the behavior of $\langle p_T \rangle$ as a function of rapidity, and show these results in Fig. 14. The corresponding πNe and πp data once more exhibit almost identical behavior. The data also reveal some interesting trends. Kinematical limitations apparently restrict $\langle p_T \rangle$ for very small and very large rapidities. For the unfavored pions, $\langle p_T \rangle$ is roughly symmetric about $y^* = 0$. For $y^* < 0$, the $\langle p_T \rangle$ values for favored and unfavored pions are similar, but for $y^* > 0$, they are

considerably larger for the favored pions. The differences seen for $y^* > 0$ are evidently due to leading particle effects in both the πp and πNe data.

In summary, the most significant differences at 10.5 GeV/c between the inclusive pion distributions from πNe and πp interactions occur in the target fragmentation region. The enhancement of charged pion production in this region stems from events which have large N_h values and which generally involve multiple collisions within the nucleus. These features are compatible with the notion that the incident hadron can undergo an effectively simultaneous collision with two or more nucleons in the nucleus. There are no significant differences found between the transverse momentum spectra for πNe and πp interactions. Moreover, the transverse momentum distributions for πNe appear to be independent of N_h, for $N_h > 1$.

C. Proton Distributions

It is of considerable interest to explore the proton production in hadron-nucleus interactions. At least two distinct processes for proton production from a nuclear target are expected: (1) recoil protons from πp or πn collisions inside the nucleus (having laboratory momentum, $p \lesssim 1.5$ GeV/c), and (2) "spectator" protons ejected by Fermi motion (having $p \lesssim 0.3$ GeV/c). Whether or not other proton production mechanisms act in hadron-nucleus collisions is an important question. We note that the presence of (fast-knock-out) protons among the shower tracks (see Sect. III. B) does suggest that such mechanisms must exist.

The reader is reminded that there are substantial losses of low momentum proton tracks below about 0.25 GeV/c (see Sect. II. B). Although

no corrections have been made for these losses, they are confined to well-defined kinematical regions.

In order to examine proton production, it is necessary to determine the characteristics of the unidentified energetic protons as well as those of the identified protons. Throughout this section, the isospin subtraction technique discussed in Sect. IV. A is used to determine the proton distribution of interest. In Fig. 15, for example, we display the p_L distributions for the positive and negative shower particles (denoted by s^+ and s^-, respectively). The difference between these distributions is equal to the p_L distribution for the unidentified protons. It can be seen in these plots that the p_L distribution for protons extends out to $p_L \sim 5$ GeV/c; this occurs both for $\pi^+ Ne \rightarrow pX$ and for $\pi^- Ne \rightarrow pX$.

The inclusive proton distributions in p_T^2 are shown in Fig. 16, and the values for $\langle p_T \rangle$ and $\langle p_T^2 \rangle$ are given in Table XI. The $\pi^+ Ne$ and $\pi^- Ne$ results agree within the experimental uncertainties.

In Fig. 17, we display the inclusive proton rapidity distributions. These distributions have been extracted from the p_L and p_T^2 data. In the region $y < 0$, which is entirely in the target fragmentation region, the distributions rise very sharply with y, approximately as $d\sigma/dy \sim e^{4y}$. For $y > 0$, the distributions fall more slowly, approximately as $d\sigma/dy \sim e^{-1.3y}$. We also note that $6 \pm 2\%$ of the protons are produced with a rapidity corresponding to $y^* > 0$.

In Fig. 18 we show the inclusive proton spectrum for laboratory

momentum, p, summed over all produced protons. The sub-histograms for identified protons are shaded. The distributions for both reactions fall rapidly with increasing momentum, but the proton tracks persist out to ~ 5 GeV/c. For $p < 1$ GeV/c, there are more protons produced in π^+Ne interactions than in π^-Ne interactions. It is probable that this difference arises from a combination of π-nucleon reaction effects, such as differing rates for Δ^{++} production and charge exchange for $\pi^+ p$. On the other hand, for $p > 1$ GeV/c, the proton spectra from the two reactions are the same within the experimental uncertainties.

It is also interesting to look for a correlation between the shower multiplicity, n_s, and the total momentum carried away by nucleons in a πNe collision. A significant correlation of this type is expected in view of the observed multiplicity correlations between n_π and N_p (see Sect. III). The averages of the longitudinal momentum per event carried by charged shower particles ($s^\pm$) and identified slow protons (p_s), as a function of n_s, are displayed in Fig. 19. The requirements of charged symmetry imply that the average longitudinal momentum per event carried by protons is given by:

$$\langle p_L(p) \rangle_{\pi^+ Ne} = \langle p_L(s^+) \rangle_{\pi^+ Ne} - \langle p_L(s^-) \rangle_{\pi^+ Ne} + \langle p_L(p_s) \rangle_{\pi^+ Ne} .$$

This expression is strictly true only for inclusive averages (i.e., when summed over n_s), but it is approximately valid for each n_s category provided that the average number of energetic protons per event is equal to the average number of energetic neutrons per event, a condition which is reasonably satisfied for $n_s \lesssim 4$.

Table XII gives the results for the partition of longitudinal momentum per event carried by π^+, π^-, π^o, p, n, Λ^o, and K^o, as obtained by the method outlined in the preceding paragraph. The fraction of longitudinal momentum taken away by protons, shown in Fig. 20, is seen to grow dramatically from 5 ± 1% for n_s = 2 to 21 ± 2% for n_s = 8. It seems remarkable that an average of approximately 40% of the incident momentum is acquired by the produced nucleons in high multiplicity ($n_s \sim 8$) collisions. It is clear that in many individual cases the fraction received by the produced nucleons must substantially exceed this average. These spectacular collisions certainly merit further experimental and theoretical investigation.

We find that the spectrum of momentum transfer to nucleons observed in πNe interactions cannot be understood in terms of a sum of independent π-nucleon collisions inside the nucleus. On the basis of the $\pi^+ p$ data near 15 GeV/c of Pisello[39] and Delay et al.,[40] we have deduced a nucleon momentum spectrum for π-nucleon collision at 10.5 GeV/c.[41] From this spectrum, we estimate that one, two, or three independent collisions inside the nucleus would transfer an average total of 0.7, 1.4, or 2.1 GeV/c to the struck nucleons, respectively. For the low multiplicity events ($n_s \leq 5$) which are presumably dominated by cases of one or two collisions, this procedure estimates that an average of 0.9 GeV/c should be transferred to the nucleons, whereas 1.7 GeV/c is observed. For the high multiplicity events ($n_s > 5$) which are presumably dominated by cases of two or more collisions, we estimate that an average of 1.7 GeV/c should

be transferred to the nucleons, whereas 3.8 GeV/c is observed. Our estimates are probably over-estimates of the probability of transferring a given amount of momentum since we do not take into account the loss of primary energy by the projectile in successive collisions. In addition, the high multiplicity events comprise nearly 30 % of the total sample whereas the independent collision procedure estimates that the probability of transferring more than 3.8 GeV/c is only 2.5 %.

We can only speculate on the mechanisms for efficiently transferring momentum to the nucleons. Because the interactions of pions with nucleons in a nucleus are always in some sense multi-nucleon collisions, this might give rise to larger than anticipated momentum transfers. It is also probable that there is some type of cascading which enhances nucleon production at wide angles in the laboratory. Another possibility is that the projectile "fireball" may have quantum numbers that would make it easily absorbable by the nucleons. It is also possible that the quark structure of the projectile is altered and is apparent in the short-time interval of the traversal of the nucleus. Clearly, this phenomenon warrants further investigation. In this regard, we note that a combined study of $\pi^+ d$ and $\pi^- d$ interactions, using the isospin symmetry requirements discussed above, would allow a complete measurement of the inclusive proton production in $\pi^{\pm} p$ interactions. It would be of particular interest to explore, as a function of A and of beam energy, the properties of protons produced with momenta above ~ 2 GeV/c.

V. NEUTRAL PARTICLE PRODUCTION

A. Neutral Pion Production

We have studied π^0 production in πNe interactions by examining the e^+e^- pairs converted from γ-rays. As discussed in Section II, each γ conversion is assigned a weight based on the chamber geometry and the conversion length in the H_2Ne mixture. Further details of the analysis techniques used may be found in Refs. 26 and 30. In what follows, we assume that all observed γ rays are produced by the decay of π^0 mesons, and we have combined the π^0 data from the isospin-symmetric reactions, $\pi^\pm Ne \rightarrow \pi^0 X$.

The π^0 multiplicity distribution is shown in Fig. 21. This distribution has been extracted from the observed γ-ray multiplicity distributions in the reactions:

$$\pi^\pm Ne \rightarrow n_\gamma \gamma + \text{anything},$$

where n_γ is the number of γ-ray conversions observed in the event ($n_\gamma \leq 6$ in the present experiment). The methods used to extract $\sigma(n_{\pi^0})$ from $\sigma(n_\gamma)$ are outlined in Refs. 26 and 30. For comparison, we also show in Fig. 21 the multiplicity distributions for charged pions in πNe interactions. The behavior of $\sigma(n_{\pi^0})$ versus n_{π^0} appears to be intermediate between that of the favored and unfavored charged pion multiplicites. The average number of π^0 mesons produced per πNe interactions, $\langle n_{\pi^0} \rangle = 1.77 \pm 0.05$, may be compared to the corresponding averages for favored pions, 2.08 ± 0.02, and unfavored pions, 1.37 ± 0.02 (see Table II). We therefore observe

an approximate equality, $\langle n_{\pi^0} \rangle \simeq 1/2 \, (\langle n_{\pi^+} \rangle + \langle n_{\pi^-} \rangle)$, as has been noted previously in π^-C interactions[8] and in pp interactions[42,43] in this energy region. The ratio of average π^0 multiplicity from πNe to that from pp is $R(\pi^0) = \langle n_{\pi^0} \rangle_{\pi Ne} / \langle n_{\pi^0} \rangle_{pp} = 1.09 \pm 0.06$, a value which is in good agreement with the charged pion multiplicity result (see Table III).

The inclusive single-π^0 distributions have been determined from the inclusive single-γ processes:

$$\pi^{\pm} Ne \rightarrow \gamma + \text{anything}.$$

In Fig. 22, the longitudinal momentum distribution of the produced γ-rays is displayed. The solid curve imposed is the result of a fit made to obtain a smooth representation of the data.[44] The dashed curves provide upper and lower uncertainty estimates for this smooth representation. Following the method of Glasser,[46] we have determined the π^0 longitudinal momentum spectrum by differentiating this smooth curve. The result is shown as the solid curve in Fig. 23. The corresponding charged pion p_L distributions are also included for comparison. It is interesting to note that, over nearly the entire p_L region, the π^0 distribution lies below that of the favored pions but above that of the unfavored pions.

A comparison between the rapidity distributions for the neutral and charged pions is shown in Fig. 24. The π^0 rapidity spectrum is approximate and has been determined from the p_L distribution together with the assumption that (for each p_L bin) the p_T^2 distributions for neutral pions and

unfavored pions are identical. We again see that the π^0 distribution is bracketed by the charged pion distributions.

We conclude that the properties of π^0 production are similar to, but intermediate between, those of the favored and unfavored charged pions in πNe interactions. The relationship between neutral and charged pion production in πNe interactions is thus similar to that found for πp interactions in this energy region.[30,42]

B. Neutral Strange Particle Production

We have determined the average multiplicities of K^0(or $\bar{K}^0$) and Λ^0 (or Σ^0) particles by observing their decays in flight. The results presented here are based on a sample of 214 V^0 decays. As discussed in Section II, each accepted V^0 was weighted for detection efficiency in the finite chamber. Corrections have also been applied for decay modes involving all neutral particles. No separation was attempted between Λ^0 and Σ^0 hyperons.

The average neutral strange particle multiplicities found in this experiment are given in Table XIII. Within the rather large uncertainties, the K^0 production from πNe appears to be equal to that from πp. The Λ^0/Σ^0 production from πNe is somewhat larger than that from πp, although the uncertainties are again rather large.

The ratios of $(K^0 + \bar{K}^0)/(\pi^+ + \pi^-)$ production, given in Table XIV are in agreement between the πp and πNe interactions. These values also agree well with previously reported results in π^+p interactions in this energy region.[47]

Note that isospin symmetry implies that

$$\sigma(\pi^{+}Ne \rightarrow K^{+}X) = \sigma(\pi^{-}Ne \rightarrow K^{o}X),$$

and

$$\sigma(\pi^{+}Ne \rightarrow K^{-}X) = \sigma(\pi^{-}Ne \rightarrow \bar{K}^{o}X).$$

Therefore the ratios of $(K^{+} + K^{-})/(\pi^{+} + \pi^{-})$ for πNe are also given by Table XIV. Since these ratios are small, we can now justify our previous neglect of charged kaons among the charged pions (see Section II. B.).

VI. SUMMARY AND CONCLUSIONS

We have undertaken a study of πNe interactions at 10.5 GeV/c covering a wide range of particle production topics. Multiplicities and correlations for charged pions, neutral pions, protons, and neutral strange particles have been examined in some detail. The inclusive production properties of charged pions, neutral pions, and protons also have been thoroughly investigated. By studying both π^+Ne and π^-Ne interactions, we have been able to apply the principle of isospin symmetry as a powerful tool to untangle the troublesome ambiguities of particle identification between protons and positive pions. Where possible, the πNe results have been compared with the corresponding πp results.

Below, we list and comment on a number of results found in this work:

1. The ratio of the average number of charged pions produced in inelastic πNe collisions compared to that produced in πp collisions is $R_{Ne}(\pi^{\pm}) = 1.08 \pm 0.03$. For neutral pion production, a similar result is found, $R_{Ne}(\pi^{0}) = 1.09 \pm 0.06$.
2. The charged pion multiplicity distribution, when expressed in a KNO scaling form, is consistent with the distribution from 200 GeV/c πNe interactions (Fig. 4).
3. A positive correlation between $\langle N_p \rangle$ and $\langle n_\pi \rangle$ is found (Figs. 5-7).

4. The inclusive production of charged pions in πNe is two or three times as large as that for πp in the target fragmentation region, but is nearly equal to the πp result in the central region and the projectile fragmentation region (Fig. 8-10).

5. The enhancement in the target fragmentation region arises mainly from events with large values of N_h (Fig. 11). N_h (or N_p) therefore appears to be a measure of the number of struck nucleons inside the nucleus and a measure of the overall violence of the collision.

6. The leading particle effect is seen in πNe interactions but it is limited to peripheral collisions having $N_h \leq 1$ (Table IX).

7. The transverse momentum distributions of charged pions are nearly identical for πNe and πp (Figs. 12, 14, Table XI). Furthermore, the values of $\langle p_T \rangle$ show little dependence on N_h (Fig. 13).

8. The properties of π^o production are similar to, but intermediate between, π^+ and π^- production in πNe interactions (Figs. 21-24).

9. Many of the qualitative features of inclusive pion production can be understood in terms of a simple kinematical model in which the effective target mass is taken to be 1, 2, or 3 nucleon masses in 59%, 30%, and 11% of the πNe collisions, respectively (Figs. 9, 11). In this model, the enhancement of the target

fragmentation region arises from events involving multiple collisions within the nucleus.

10. Our study of inclusive proton production covers the complete kinematical region, except for $p \lesssim 0.25$ GeV/c. A rather large fraction of the produced protons are too energetic in the laboratory ($p \gtrsim 1.3$ GeV/c) to be visually identified by track density (Figs. 1, 15-18).

11. The average fraction of the incident momentum that is carried away by nucleons rises sharply with the shower-track multiplicity, from approximately 10% for $n_s = 2$ to approximately 40% for $n_s = 8$ (Figs. 19-20, Table XII). Such large momentum transfers are not expected on the basis of known np interaction properties. This effect merits further investigation.

ACKNOWLEDGMENTS

It is a pleasure to acknowledge the assistance given to us at the Stanford Linear Accelerator Center by R. Gearhart, R. Watt, and the 82-inch bubble chamber staff. We are also grateful for the efforts of our scanning and measuring staffs.

APPENDIX A. Details of the Fitting Procedure Used to Find the Corrected Multiplicity Distributions

In this Appendix, we provide details of the fitting procedure outlined in Section III. B. In order to simplify the notation, we use

$$i = n_{+} \quad ,$$

$$j = n_{\pi^+} \quad ,$$

and

$$k = n_{-} = n_{\pi^-} \quad .$$

Other notation, unless defined here, is the same as in Section III.

In the least-squares fit we have defined χ^2 as follows:

$$\chi^2 = \chi_1^2 + \chi_2^2 + \chi_3^2 \quad ,$$

where

$$\chi_1^2 = \sum_j \sum_k \left(\frac{H^+(j,k) - H^-(k,j)}{\delta H(j,k)} \right)^2$$

$$\chi_2^2 = \left(\frac{\langle j+k \rangle_{\pi^+ Ne^-} - \langle n_\pi \rangle}{\delta \langle n_\pi \rangle} \right)^2 + \left(\frac{\langle j+k \rangle_{\pi^- Ne^-} - \langle n_\pi \rangle}{\delta \langle n_\pi \rangle} \right)^2 \quad ,$$

$$\chi_3^2 = \left(\frac{\bar{\Delta}_\pi(\pi^+ Ne) - \bar{\Delta}_\pi(\pi^- Ne)}{\delta \Delta_\pi} \right)^2 \quad ,$$

$\delta H(j,k)$ = statistical error on $H^+(j,k) - H^-(k,j)$,

$\delta \langle n_\pi \rangle$ = statistical error on $\langle n_\pi \rangle$,

and

$\delta \Delta_\pi$ = statistical error on $\bar{\Delta}_\pi(\pi^\pm Ne)$.

We note that χ_1^2 enforces the constraints of charge symmetry, χ_2^2 constrains the corrected distributions to be consistent with $\langle n_\pi \rangle$ of Table III, and χ_3^2 forces the average net beam-like charge to be consistent between

the π^+Ne and π^-Ne distributions.

The parameterization used for $H^{\pm}(j,k)$ is

$$H^{\pm}(j,k) = \sum_{i=j}^{j_{max}} T^{\pm}(i,j,k)\, G^{\pm}(i,k) \quad .$$

where $T^{\pm}(i,j,k)$ is a binomial coefficient:

$$T^{\pm}(i,j,k) = \frac{i!}{j!\,(i-j)!} \left(P^{\pm}(i,k)\right)^{i-j} \left(1 - P^{\pm}(i,k)\right)^{j} \quad ,$$

and where $P^{\pm}(i,k)$ is the probability that a positive shower track is a proton. $P^{\pm}(i,k)$ is parameterized as follows:

$$P^{\pm}(i,k) = a_1^{\pm} + a_2^{\pm} i + a_3^{\pm} i^2 + a_4^{\pm} k + a_5^{\pm} k^2 \quad .$$

This formulation therefore required 10 parameters. However, in practice it was found necessary to allow more freedom in the fit, and the five probability elements, $P^+(1,0)$, $P^+(2,0)$, $P^+(2,1)$, $P^-(1,0)$, and $P^-(1,1)$ were allowed to vary independently from the functional form.

There were 52 non-zero bins in the final $H^{\pm}(j,k)$ distributions for $0 \leq j \leq 7$ and $0 \leq k \leq 7$ (i.e., 12 of the 64 possible bins had less than 1 event). A total of 55 quantities (52 for χ_1^2, 2 for χ_2^2, and 1 for χ_3^2) were thus fitted with 15 parameters. The final χ^2 was 38.3 for 40 degrees of freedom.

REFERENCES AND FOOTNOTES

[1] Recent reviews in this field include: W. Busza, Proc. of the Sixth Int. Conf. on High Energy Physics and Nuclear Structure, Los Alamos (1975); L. Bertocchi, Proc. of the Sixth Int. Conf. on High Energy Physics and Nuclear Structure, Los Alamos (1975); B. Anderssen, Proc. of the Seventh Int. Conf. on Multiparticle Reaction, Munich (1976). A survey of early work may be found in U. Camerini, W. O. Lock, and D. H. Perkins, Progress in Cosmic Ray Physics, North-Holland Publishing Co., Amsterdam (1952).

[2] J. Babecki, Z. Czachowska, B. Furmanska, J. Gierula, R. Holynski, A. Jurak, S. Krzywdzinski, G. Nowak, B. Slezak, and W. Wolter, Phys. Lett. 47B, 268 (1973); Phy. . Lett. 52B, 247 (1974).

[3] J. Hébert et al., Phys. Lett. 48B, 467 (1974).

[4] A. Gurtu, P. K. Malhotra, I. S. Mittra, P. M. Sood, S. C. Gupta, V. K. Gupta, G. L. Kaul, L. K. Mangotra, Y. Prakash, N. K. Rao, and M. K. Sharma, Phys. Lett. 50B, 391 (1974).

[5] R. E. Gibbs, J. R. Florian, L. D. Kirkpatrick, J. J. Lord, and J. W. Martin, Phys. Rev. D 10, 783 (1974); Nuovo Cim. 25A, 447 (1975).

[6] P. L. Jain, M. Kazuno, G. Thomas, and B. Girard, Phys. Rev. Lett. 33, 660 (1974); Lett.al Nuovo Cim. 12, 653 (1975); Phys. Rev. Lett. 34, 972 (1975).

[7] J. I. Cohen, E. M. Friedländer, M. Marcu, A. A. Marin, and R. Nitu, Lett. al Nuovo Cim. 9, 337 (1974).

[8] O. Balea et al., Phys. Lett. 39B, 571 (1972); Nucl. Phys. D63, 114 (1973).

[9] V. G. Grishin, T. Ya. Inogamova, and Sh. V. Inogamov, Yad. Phys. 19, 1364 (1974). (Sov. J. Nucl. Phys. 19, 697 (1974).)

[10] M. Azimova et al., Yad. Fiz. 20, 921 (1974). (Sov. J. Nucl. Phys. 20, 490 (1975).)

[11] J. R. Elliott, L. R. Fortney, A. T. Goshaw, J. W. Lamsa, J. S. Loos, W. J. Robertson, W. D. Walker, W. M. Yeager, and M. E. Binkley, Phys. Rev. Lett. 34, 607 (1975).

[12] D. J. Miller and R. Nowak, Lett. al Nuovo Cim. 13, 39 (1975).

[13] W. Busza, J. E. Elias, D. F. Jacobs, P. A. Swartz, C. C. Young, and M. R. Sogard, Phys. Rev. Lett. 34, 836 (1975).

[14] W. Busza, D. Luckey, L. Votta, C. Young, C. Halliwell, and J. Elias, MIT-Carleton-Fermilab preprint, submitted to the Eighteenth Int. Conf. on High Energy Physics, Tbilisi (1976).

[15] L. J. Gutay, A. T. Laasanen, C. Ezell, W. N. Schreiner, and F. Turkot, Phys. Rev. Lett. 37, 468 (1976).

[16] Z. Koba, H. Nielsen, and P. Olesen, Nucl. Phys. B40, 317 (1972).

[17] P. Slattery, Phys. Rev. Lett. 29, 1624 (1972).

[18] A. Dar and J. Vary, Phys. Rev. D6, 2412 (1972).

[19] P. M. Fishbane and J. S. Trefil, Phys. Rev. D 8, 1467 (1973).

[20] K. Gottfried, Proc. of the Fifth Int. Conf. on High Energy Physics and Nuclear Structure, Uppsala, Sweden (1973); Phys. Rev. Lett. 32, 957 (1974).

[21] G. Berlad, A. Dar, and G. Eilam, Phys. Rev. D 13, 161 (1976).

[22] Y. Afek, G. Berlad, G. Eilam, and A. Dar, Israel Institute of Technology report no. Technion-PH-76-48, 1976 (unpublished).

[23] Collected Papers of L. D. Landau (ed. D. Ter Haar), Pergamon Press, London (1965).

[24] W. D. Walker, Phys. Rev. Lett. 24, 1143 (1970).

[25] A. S. Goldhaber, Phys. Rev. D 7, 765 (1973); Phys. Rev. Lett. 35, 748 (1975).

[26] W. M. Yeager, Ph. D. dissertation, Duke University, 1976 (unpublished).

[27] J. C. Allaby et al., Yad. Fiz. 12, 538 (1970). (Sov. J. Nucl. Phys. 12, 295 (1971).)

[28] The central beam momentum values were found by a study of events from the nuclear coherent reactions $\pi^{\pm}Ne \rightarrow \pi^{\pm}\pi^{+}\pi^{-}Ne$. A study of K^{o}_{s} decays determined the value of the magnetic field at the center of the chamber to be 15.28 kilogauss.

[29] L. R. Fortney, Proc. of the Int. Conf. of Data Handling Systems in High Energy Physics, CERN Report 70-21, Vol. 1, p. 215 (1970); Proc. of the Oxford Conf. on Computer Scanning, Vol. 1, p. 137 (Oxford, 1974).

[30] For details on the γ conversion corrections, see J. R. Elliott, Ph. D. dissertation, Duke University, 1976 (unpublished).

[31] E. Bracci, J. P. Droulez, E. Flaminio, J. D. Hansen, and D. R. O. Morrison, Report No. CERN/HERA 72-1, 1972 (unpublished).

[32] We note that in Ref. 21, the parameter β is taken to be 0.6 which implies $\langle\nu\rangle_{Ne} \cong 3.5$. This value of $\langle\nu\rangle_{Ne}$ appears to be too large. We have used $\beta = 0.18$ in order to obtain $\langle\nu\rangle_{Ne} = 1.6$ and $\langle\nu^{1/4}\rangle_{Ne} = 1.1$.

[33] B. Andersson and I. Otterlund, Nucl. Phys. B99, 425 (1975).

[34] We used a value of 270 mb for the πNe inelastic cross section, based on an interpolation of measurements from Ref. 26. Inelastic π-nucleon cross sections have been taken from the compilation of Ref. 31.

[35] M. F. Kaplon and D. M. Ritson, Phys. Rev. 88, 386 (1952).

[36] V. Sreedhar, C.-Y. Chien, B. Cox, D. Felock, R. Zdanis, C. Bromberg, T. Ferbel, and P. Slattery, Nucl. Phys. B75, 285 (1974).

[37] The $d\sigma/dy$ distributions at energies corresponding to $y = 1, 2$, and 3 have been scaled from the $\pi^+ d \rightarrow \pi^- X$ data at 24 GeV/c (Ref. 36).

[38] J. T. Powers, N. N. Biswas, N. M. Cason, V. P. Kenney, and W. D. Shephard, Phys. Rev. D 8, 1947 (1973).

[39] D. M. Pisello, Ph. D. dissertation, Columbia University, 1976 (unpublished).

[40] M. J. Delay, K. Heller, G. Miller, H. Romer, J. E. Rothberg, A. Schenck, and R. W. Williams, Phys. Rev. D 11, 975 (1975).

[41] The data of Ref. 39 covers the region for Feynman $x < -0.2$, and the data of Ref. 40 covers the region $-0.5 < x < 0.5$. We combined these data in order to get a complete proton spectrum. This spectrum was then scaled down to 10.5 GeV/c by shrinking the range of the rapidity spectrum.

[42] N. N. Biswas, E. D. Fokitis, J. M. Bishop, N. M. Cason, V. P. Kenney, and W. D. Shephard, Phys. Rev D 10, 3579 (1974).

[43] M. E. Binkley, J. R. Elliott, L. R. Fortney, J. S. Loos, W. J. Robertson, C. M. Rose, W. D. Walker, W. M. Yeager, G. W. Meisner, and R. B. Muir, Phys. Lett. 45B, 295 (1973).

[44] The $p_L(\gamma)$ distribution was fitted in 2 momentum regions as follows:

$$\sigma_{inel}^{-1} \frac{d\sigma(\gamma)}{dp_L} = p_L^{-1} \sum_{n=0}^{5} A_n \left[\ln(2\, p_L/m_\pi)\right]^n \quad \text{for } p_L < 3 \text{ GeV/c}$$

$$= A_6 \exp(-A_7 p_L) \quad \text{for } p_L > 3 \text{ GeV/c.}$$

The lower energy form was suggested by Kopylov (Ref. 45). The fitted parameters, A_0 through A_7, are: 0.556, 0.611, -0.467, 0.270, -0.089, 0.010, 0.983 $(\text{GeV/c})^{-1}$, and 0.799 $(\text{GeV/c})^{-1}$.

[45] G. I. Kopylov, Nucl. Phys. B52, 126 (1973).

[46] R. G. Glasser, Phys. Rev. D 6, 1993 (1973).

[47] P. H. Stuntebeck, N. M. Cason, J. M. Bishop, N. N. Biswas, V. P. Kenney, and W. D. Shephard, Phys. Rev. D 9, 608 (1974).

Table I. Summary of Data Sample

Beam Particle	π^+	π^-
Avg. beam momentum (GeV/c)	10.46	10.39
Number photographs analyzed	26,600	25,800
Number events observed	13,360	16,268
Number πNe events expected[a]	9,620 (72%)	12,225 (71%)
Number πp events expected[a]	3,740 (28%)	4,043 (29%)
Number of events classified as neonic[b]	7,752 (58%)	8,904 (55%)
Number of events classified as hydrogenic[b]	5,608 (42%)	7,364 (45%)

a. The liquid mixture in the bubble chamber consisted of 32 molar percent Ne and 68 molar percent H_2. The inelastic πNe cross section is taken to be 270 mb (See Ref. 27).

b. A scanned event was classified as "hydrogenic" if it had 0 or 1 identified proton track and net charge consistent with a πp collision. Otherwise it was classified as "neonic." As noted in the text, some collisions involving a peripheral proton from a Ne nucleus were classified as hydrogenic.

Table II. Averaged charged particle multiplicities in $\pi^{\pm}$ Ne interactions at 10.5 GeV/c

Reaction	Averages						
	$\langle n_- \rangle$	$\langle n_- \rangle$	$\langle N_h \rangle$	$\langle n_{ch} \rangle$	$\langle n_{\pi^-} \rangle^a$	$\langle n_{\pi^-} \rangle^a$	$\langle N_p \rangle^a$
π^+Ne	2.80 ± 0.04	1.37 ± 0.02	1.71 ± 0.09	5.94 ± 0.10	2.08 ± 0.02	1.37 ± 0.02	2.49 ± 0.10
π^-Ne	1.83 ± 0.02	2.08 ± 0.02	1.50 ± 0.08	5.41 ± 0.09	1.37 ± 0.02	2.08 ± 0.02	1.96 ± 0.09

a. It is assumed that $\langle n_{\pi^-} \rangle \approx \langle n_- \rangle$. The values for $\langle n_{\pi^+} \rangle$ and $\langle N_p \rangle$ then follow from isotopic spin symmetry (see text).

Table III. Charged-pion-multiplicity distribution parameters for inelastic πNe interactions and comparison to inelastic πp interactions at 10.5 GeV/c.

Reaction	$\langle n_\pi \rangle^{a,b}$	$R = \frac{\langle n_\pi \rangle_{\pi Ne}}{\langle n_\pi \rangle_{\pi p}}$	Dispersion $\left(\langle n_\pi^2 \rangle - \langle n_\pi \rangle^2\right)^{\frac{1}{2}}$
$\pi^{\pm}$Ne	3.45 ± 0.05		1.99 ± 0.03
$\pi^+ p^c$	3.33 ± 0.07	1.04 ± 0.03	
$\pi^- p^c$	3.12 ± 0.07	1.11 ± 0.03	

a. Elastic events have been removed from all interactions.

b. Proton tracks have been removed from the πNe data by the requirements of charge symmetry, as discussed in the text. Proton tracks have been deleted from the πp data by assuming an average of 0.65 or 0.60 proton per inelastic $\pi^+ p$ or $\pi^- p$ interactions, respectively.

c. Interpolated from the compilation of Ref. 31.

Table VI. (continued)

B. π^- Ne Interactions

n_π	N_p											
	0	1	2	3	4	5	6	7	8	9	10	11
0	127	44	16	9	6	4	2	1			1	
1	799	500	219	96	44	27	14	8	3			
2	580	359	239	158	75	47	28	15	5	5		
3	633	534	336	217	132	97	57	26	13	5	1	1
4	414	370	311	231	152	108	65	42	19	8	4	2
5	205	250	251	168	147	99	74	36	19	12	6	2
6	124	133	122	114	91	76	49	34	20	11	3	2
7	40	61	63	61	53	47	34	23	15	4	3	2
8	19	27	26	27	29	25	19	15	5	4	3	
9	6	8	12	15	12	12	10	5	3	3		
10	2	3	5	5	7	5	4	2	1			
11	1	1	2	2	2	2	2	1				
12			1	1	1	1						
13					1							

Table V. Event populations for inelastic $\pi^{\pm}$Ne interactions corrected for the presence of misidentified proton tracks. The π^{-}Ne results are tabulated within parentheses below the corresponding π^{+}Ne results. Both samples are normalized to 10 000 events to facilitate comparison. The number of π^{+} or π^{-} tracks per event are denoted by n_{π^+} or n_{π^-}, respectively. Events arising from πp interactions have been subtracted.

n_{π^-} for π^+Ne or (n_{π^+} for π^-Ne)	n_{π^+} for π^+Ne or (n_{π^-} for π^-Ne)							
	0	1	2	3	4	5	6	7
0	202 (210)	1564 (1627)	402 (419)	76 (87)	12 (14)	1 (2)		
1	137 (83)	1044 (1075)	1812 (1672)	650 (583)	104 (113)	11 (16)	1 (1)	
2	29 (18)	308 (287)	910 (1071)	898 (917)	327 (272)	51 (55)	5 (5)	
3	5 (7)	58 (58)	235 (229)	380 (449)	272 (256)	86 (79)	13 (12)	1 (1)
4	2 (1)	10 (8)	42 (40)	90 (88)	100 (100)	54 (52)	14 (12)	2 (2)
5	1 (0)	2 (0)	9 (5)	23 (14)	26 (20)	17 (18)	6 (6)	1 (1)
6			1 (1)	2 (2)	3 (4)	2 (5)	1 (1)	0 (1)
7					0 (1)	0 (1)		

Table III. Charged-pion-multiplicity distribution parameters for inelastic πNe interactions and comparison to inelastic πp interactions at 10.5 GeV/c.

Reaction	$\langle n_\pi \rangle$ [a, b]	$R = \frac{\langle n_\pi \rangle_{\pi Ne}}{\langle n_\pi \rangle_{\pi p}}$	Dispersion $\left(\langle n_\pi^2 \rangle - \langle n_\pi \rangle^2\right)^{\frac{1}{2}}$
π^+Ne	3.45 ± 0.05		1.99 ± 0.03
$\pi^+ p$ [c]	3.33 ± 0.07	1.04 ± 0.03	
$\pi^- p$ [c]	3.12 ± 0.07	1.11 ± 0.03	

a. Elastic events have been removed from all interactions.

b. Proton tracks have been removed from the πNe data by the requirements of charge symmetry, as discussed in the text. Proton tracks have been deleted from the πp data by assuming an average of 0.65 or 0.60 proton per inelastic $\pi^+ p$ or $\pi^- p$ interactions, respectively.

c. Interpolated from the compilation of Ref. 31.

Table VII. Multiplicity distributions of charged shower particles and charged pions. n_s is the number of shower particles per event uncorrected for the presence of unidentified proton tracks; n_π is the number of charged pions per event corrected for the misidentified proton tracks. The distributions are normalized to 10 000 events.

	No. Uncorrected Events			No. Corrected Events	
n_s	π^+ Ne	π^- Ne	n_π	π^+ Ne	π^- Ne
0	77 ± 9	210 ± 33	0	202 ± 23	210 ± 33
1	1297 ± 63	1400 ± 70	1	1701 ± 73	1710 ± 77
2	1198 ± 57	1488 ± 67	2	1475 ± 68	1511 ± 66
3	1769 ± 87	1684 ± 82	3	2201 ± 96	2052 ± 91
4	1604 ± 87	1617 ± 84	4	1632 ± 68	1726 ± 74
5	1332 ± 47	1186 ± 41	5	1248 ± 46	1269 ± 44
6	1054 ± 46	1033 ± 42	6	761 ± 33	779 ± 32
7	655 ± 26	575 ± 22	7	422 ± 21	406 ± 18
8	455 ± 23	397 ± 18	8	214 ± 15	199 ± 13
9	233 ± 15	219 ± 13	9	95 ± 10	86 ± 8
10	158 ± 13	99 ± 9	10	36 ± 6	34 ± 5
11	101 ± 10	60 ± 7	11	10 ± 3	13 ± 3
12	44 ± 7	22 ± 4	12	2 ± 1	4 ± 2
13	21 ± 5	6 ± 2	13		1 ± 1

Table IX. Average number of favored and unfavored pions produced in various kinematical regions.

Kinematical Regions	n_{π^-} per event		Average number excess favored pions per event
	π^- Ne	π^+ Ne	
$y < 1$ (target)			
$N_h \leqslant 1$ (peripheral)	0.24 ± 0.01	0.16 ± 0.01	0.08 ± 0.02
$N_h \geqslant 2$ (non-peripheral)	0.34 ± 0.01	0.28 ± 0.01	0.06 ± 0.02
$1 < y < 2.2$ (central)			
$N_h \leqslant 1$ (peripheral)	0.48 ± 0.02	0.28 ± 0.01	0.20 ± 0.02
$N_h \geqslant 2$ (non-peripheral)	0.39 ± 0.01	0.33 ± 0.01	0.06 ± 0.02
$y > 2.2$ (projectile)			
$N_h \leqslant 1$ (peripheral)	0.41 ± 0.02	0.18 ± 0.01	0.23 ± 0.02
$N_h \geqslant 2$ (non-peripheral)	0.23 ± 0.01	0.14 ± 0.01	0.09 ± 0.02

Table XI. Transverse momentum averages for πNe and πp interactions at 10.5 GeV/c.

Reaction	$\langle p_T \rangle$ GeV/c	$\langle p_T^2 \rangle$ (GeV/c)^2
$\pi^+ Ne \rightarrow \pi^- X$	0.309 ± 0.004	0.158 ± 0.005
$\pi^- Ne \rightarrow \pi^- X$	0.348 ± 0.004	0.187 ± 0.005
$\pi^+ p \rightarrow \pi^- X$	0.306 ± 0.006	0.139 ± 0.007
$\pi^- p \rightarrow \pi^- X$	0.368 ± 0.006	0.198 ± 0.008
$\pi^+ Ne \rightarrow p X$ [a]	0.395 ± 0.008	0.214 ± 0.008
$\pi^- Ne \rightarrow p X$ [a]	0.401 ± 0.008	0.238 ± 0.008

a. Corrected to include energetic, unidentified, protons. The correction procedure uses the requirements of isotopic spin symmetry as discussed in the text. Protons having laboratory momenta below 0.2 GeV/c are *omitted from these averages.*

Table XIII. Average multiplicities of neutral strange particles. The results have been corrected for neutral decay modes, finite chamber volume, and other inefficiencies.

	πNe		πp	
Beam	K^0 and $\bar{K}^0$	Λ^0 and Σ^0	K^0 and $\bar{K}^0$	Λ^0 and Σ^0
π^+	0.10 ± 0.02	0.07 ± 0.01 [a]	0.07 ± 0.02	0.03 ± 0.01
π^-	0.14 ± 0.03		0.14 ± 0.04	0.05 ± 0.02

a. Averaged over the isospin-symmetric π^+Ne and π^-Ne interactions.

Table XIV. Ratio of $(K^0 + \bar{K}^0)/(\pi^+ + \pi^-)$ production.

Beam	πNe	πp
π^+	0.029 ± 0.005	0.022 ± 0.006
π^-	0.040 ± 0.008	0.043 ± 0.010

Fig. 3. Distribution of the net charge, Δ_π, of the pion tracks from πNe interactions at 10.5 GeV/c, averaged over π^+Ne and π^-Ne interactions, and normalized to 10 000 events. Δ_π is defined in the caption for Fig. 1. Proton tracks have been removed (see text). The dashed curves illustrate an approximate exponential fall-off for both positive and negative values of Δ_π.

Fig. 4. *Distributions of the corrected number of protons per event* in π^+Ne (solid histogram) and π^-Ne (dashed histogram) interactions at 10.5 GeV/c. Both histograms are normalized to 10 000 events.

Fig. 5. (a) Average charged pion multiplicity versus N_p for π^+Ne (●) and π^-Ne (▼) interactions at 10.5 GeV/c.

(b) Ratio of the dispersion parameter divided by the average charged pion multiplicity as a function of N_p.

Fig. 6. Average proton multiplicity versus n_π for π^+Ne (●) and π^-Ne (▼) interactions at 10.5 GeV/c.

Fig. 7. (a) Average charged pion multiplicity versus the number of fast knockout protons, N_f.

the number of nucleons participating in the collision. The rapidity boosts, $\xi_{\pi\nu}$, between the laboratory and the center-of-mass of the incident pion and ν nucleons are indicated by the vertical arrows. *See text for a more complete explanation.*

Fig. 12. Distributions in p_T^2 for πNe (solid histograms) and πp (dashed histograms) interactions. (a) Favored pions. (b) Unfavored pions. The data are normalized so that equal numbers of tracks are plotted for πp and πNe.

Fig. 13. Average values of the transverse momentum as a function of N_h. The solid (open) symbols refer to πNe (πp) interactions. The triangles (circles) are for the favored (unfavored) pions. The diamonds represent the values found for the most energetic favored pion.

Fig. 14. Average values of the transverse momentum as a function of rapidity. (a) πNe interactions. (b) πp interactions.

Fig. 15. Distributions in longitudinal momentum for (a) favored and (b) unfavored shower particles. *The solid (dashed)* histograms are for the positively (negatively) charged shower particles, as indicated. The longitudinal momentum distribution for unidentified protons is obtained by the difference (solid minus dashed) between the plotted distributions.

Fig. 21. π^0 multiplicity distribution in πNe interactions at 10.5 GeV/c (■). The charged pion multiplicity distributions at this energy are also shown for favored pions (▽) and unfavored pions (○).

Fig. 22. Inclusive longitudinal momentum distribution for γ-rays produced in the process π^+Ne → γX at 10.5 GeV/c. The solid curve is a smooth representation of the data; the dashed curves provide uncertainties in this smooth representation.

Fig. 23. Inclusive longitudinal momentum distribution for π^0 from $\pi^\pm$Ne → π^0X (smooth curve) compared to those for charged pions from π^-Ne → π^-X (solid histogram) and from π^+Ne → π^-X (dashed histogram). The π^0 distribution has been obtained from the smooth representation of the γ distribution (preceding figure) by using the method of Ref. 46.

Fig. 24. Inclusive rapidity spectrum for π^0 from $\pi^\pm$Ne → π^0X (smooth curve) compared to those for charged pions from π^-Ne → π^-X (solid histogram) and from π^+Ne → π^-X (dashed histogram).

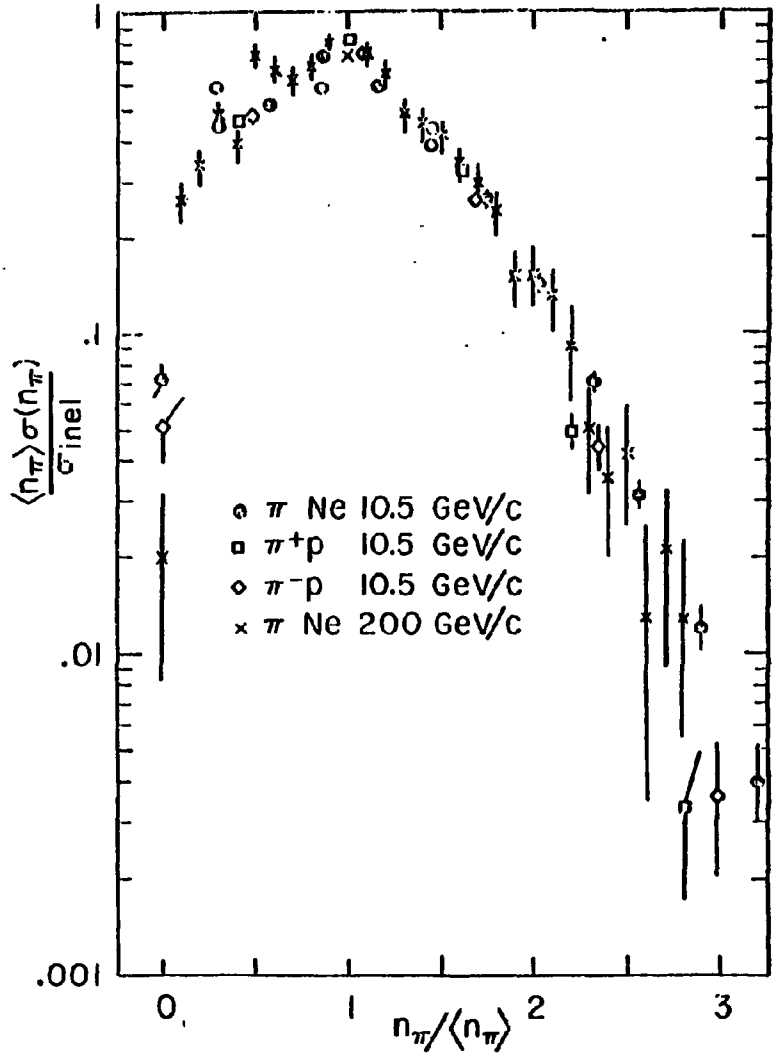
1
.1
.01
.001
0
1
2
3
$\frac{\langle n_\pi \rangle \sigma(n_\pi)}{\sigma_{inel}}$
$n_\pi/\langle n_\pi \rangle$
π Ne 10.5 GeV/c
π⁺p 10.5 GeV/c
π⁻p 10.5 GeV/c
π Ne 200 GeV/c

Fig. 2.

Fig. 1

Fig. 4

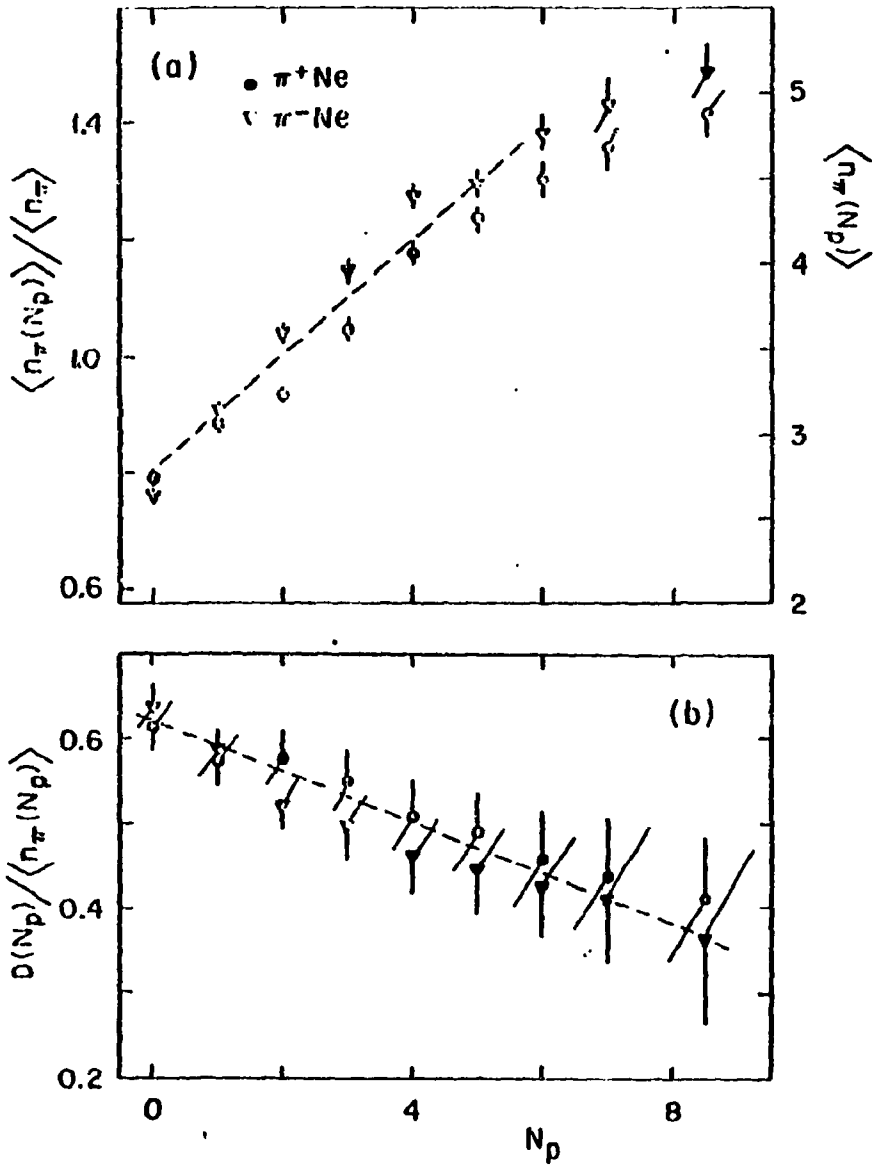

Fig. 5.

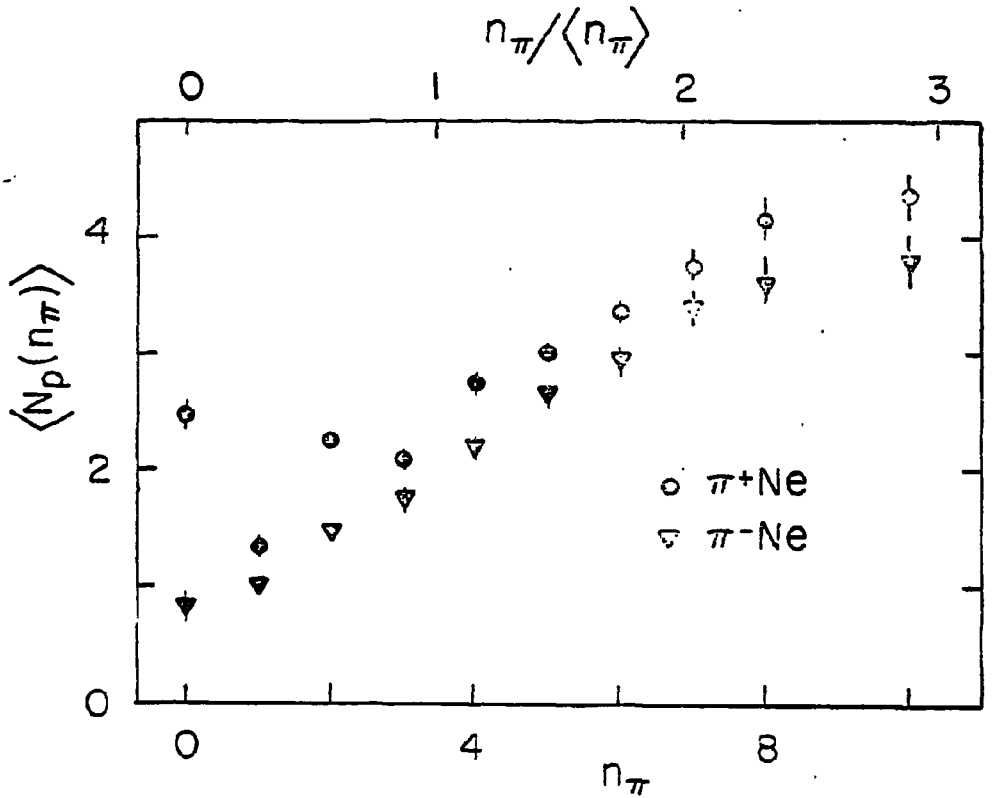
$n_\pi/\langle n_\pi \rangle$
0
1
2
3
$\langle N_p(n_\pi) \rangle$
0
2
4
π+Ne
π-Ne
0
4
8
n_π

Fig. 6

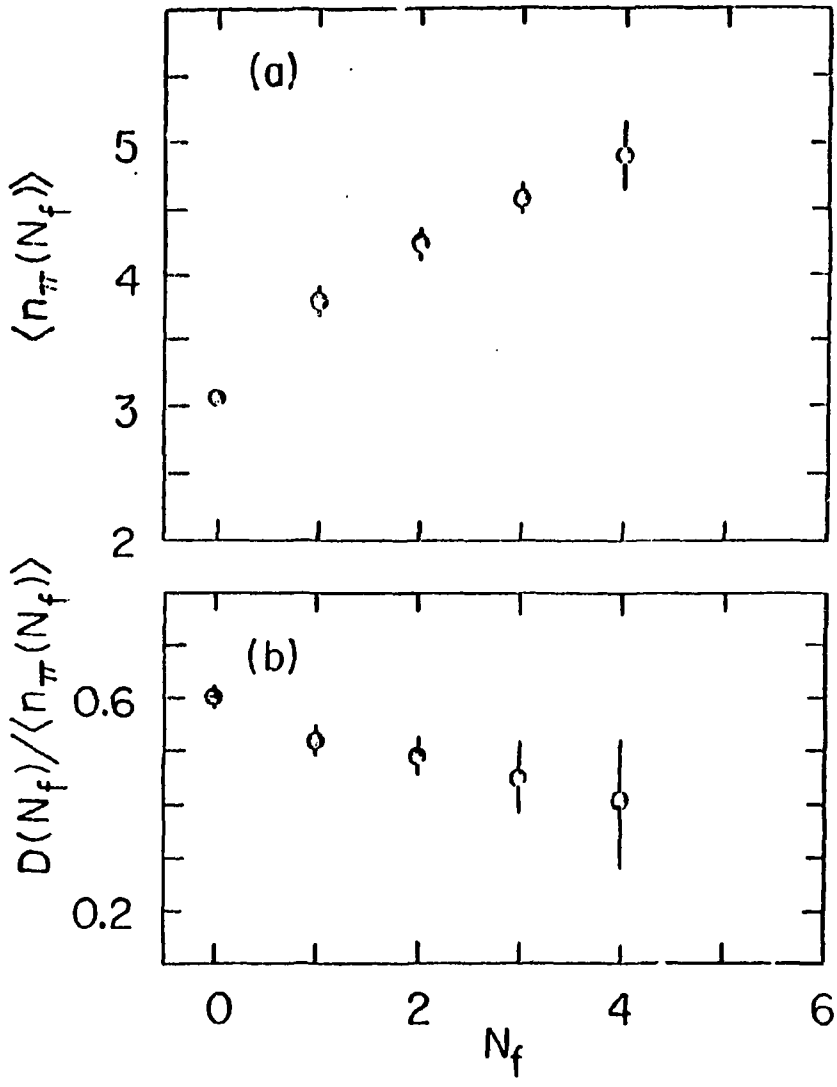
(a)
$\langle n_\pi(N_f)\rangle$
5
4
3
2
(b)
$D(N_f)/\langle n_\pi(N_f)\rangle$
0.6
0.2
0
2
4
6
N_f

Fig. 7

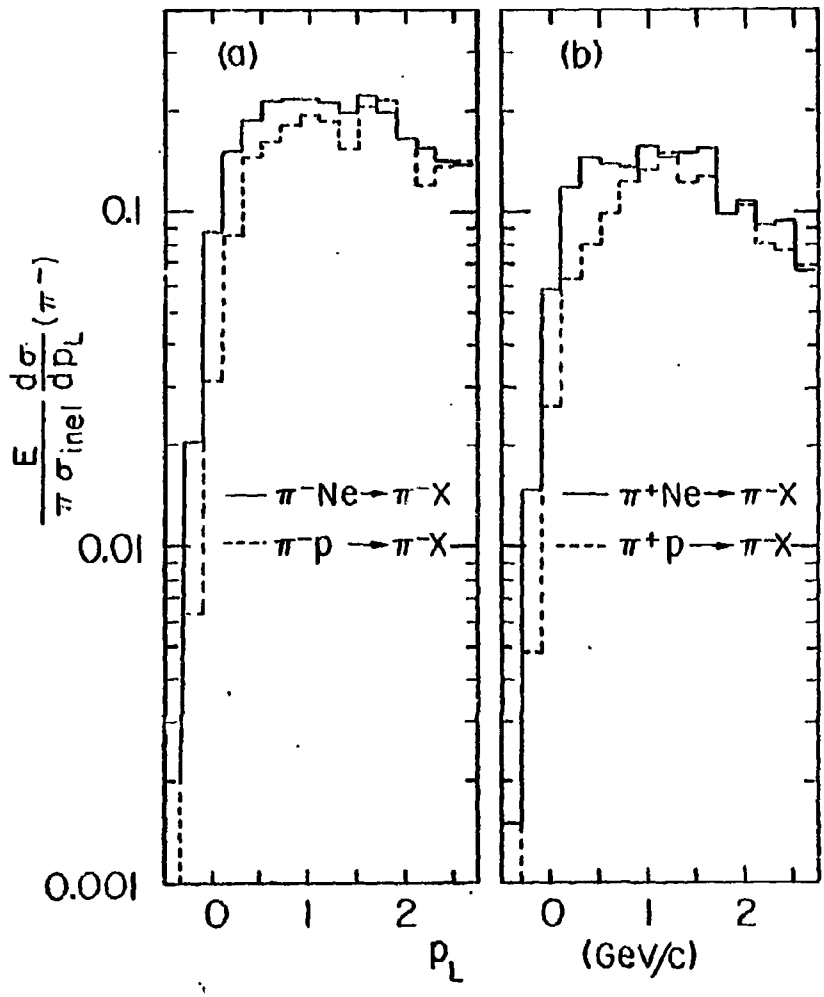
(a)
(b)
0.1
0.01
0.001
$\frac{E}{\pi\,\sigma_{inel}}\frac{d\sigma}{dp_L}(\pi^-)$
$\pi^-Ne \rightarrow \pi^-X$
$\pi^-p \rightarrow \pi^-X$
$\pi^+Ne \rightarrow \pi^-X$
$\pi^+p \rightarrow \pi^-X$
0
1
2
p_L
(GeV/c)

Fig. 8.

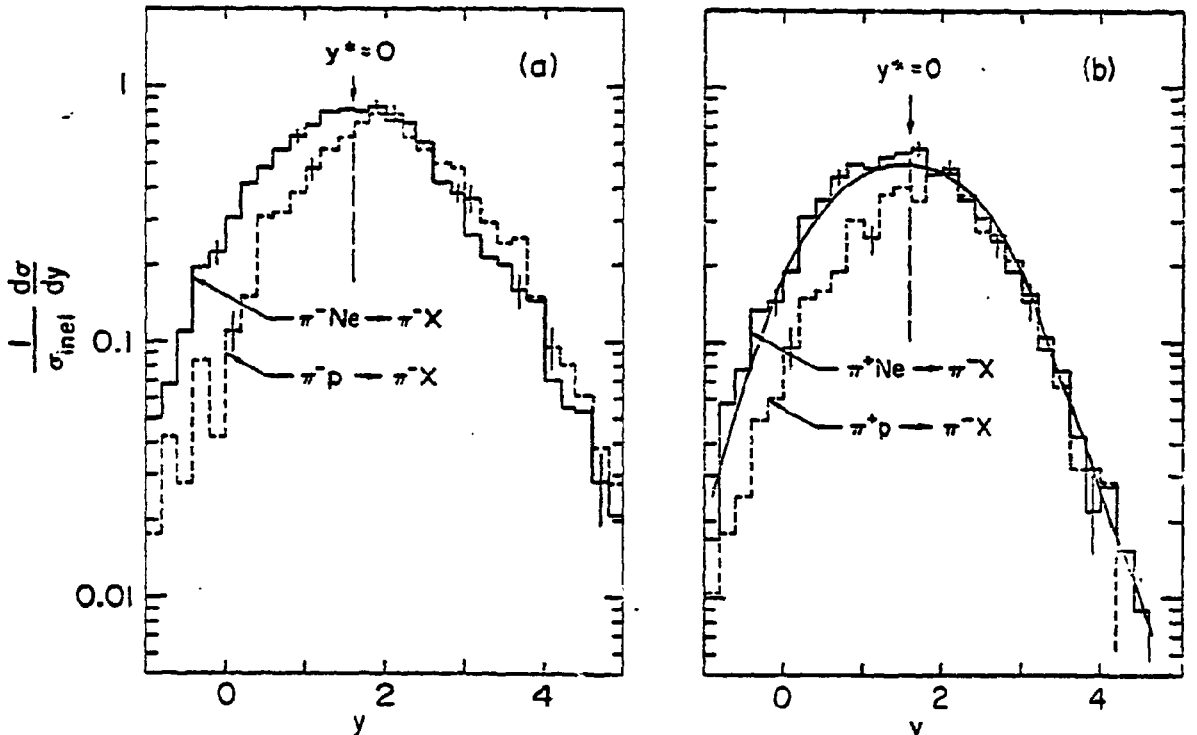
y*=0
(a)
1
0.1
0.01
$\frac{1}{\sigma_{inel}}\frac{d\sigma}{dy}$
$\pi^-Ne \rightarrow \pi^-X$
$\pi^-p \rightarrow \pi^-X$
0
2
4
y
y*=0
(b)
$\pi^+Ne \rightarrow \pi^-X$
$\pi^+p \rightarrow \pi^-X$
0
2
4
y

$\frac{\sigma_{inel}(\pi p)}{\sigma_{inel}(\pi Ne)} \frac{d\sigma}{dy}(\pi Ne \to \pi^- X)$
$\frac{d\sigma}{dy}(\pi p \to \pi^- X)$
0
2
4
y
$y^*=0$
π^+beam
π^-beam

Fig. 10.

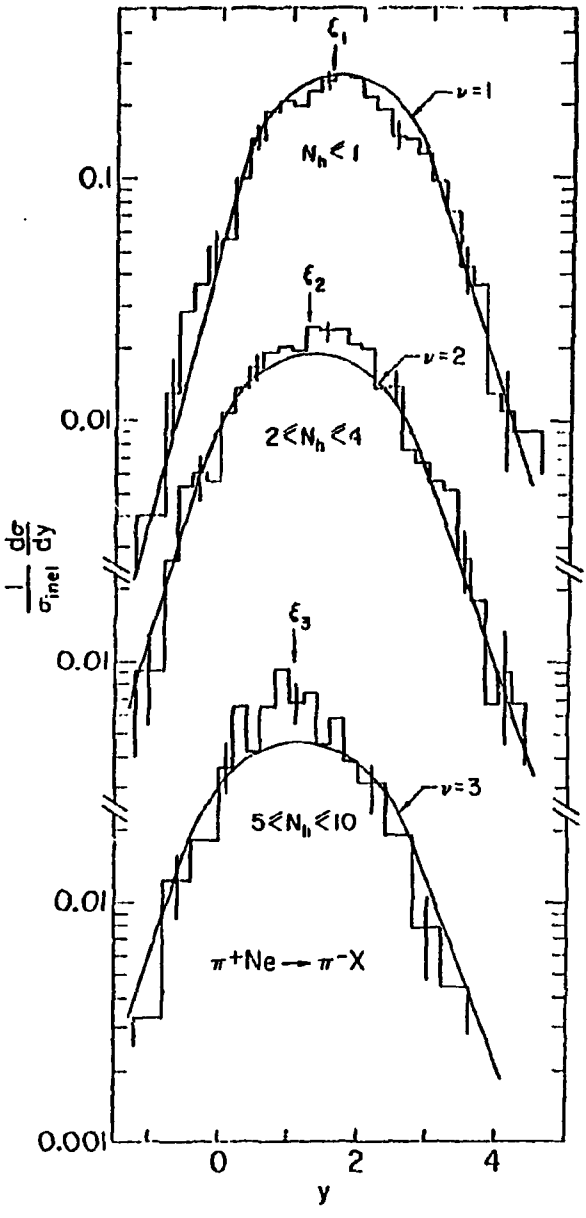
ξ_1
$\nu=1$
$N_h \leq 1$
0.1
ξ_2
$\nu=2$
0.01
$2 \leq N_h \leq 4$
$\frac{1}{\sigma_{inel}} \frac{d\sigma}{dy}$
ξ_3
0.01
$\nu=3$
$5 \leq N_h \leq 10$
0.01
$\pi + Ne \rightarrow \pi^- X$
0.001
0
2
4
y

Fig. 11

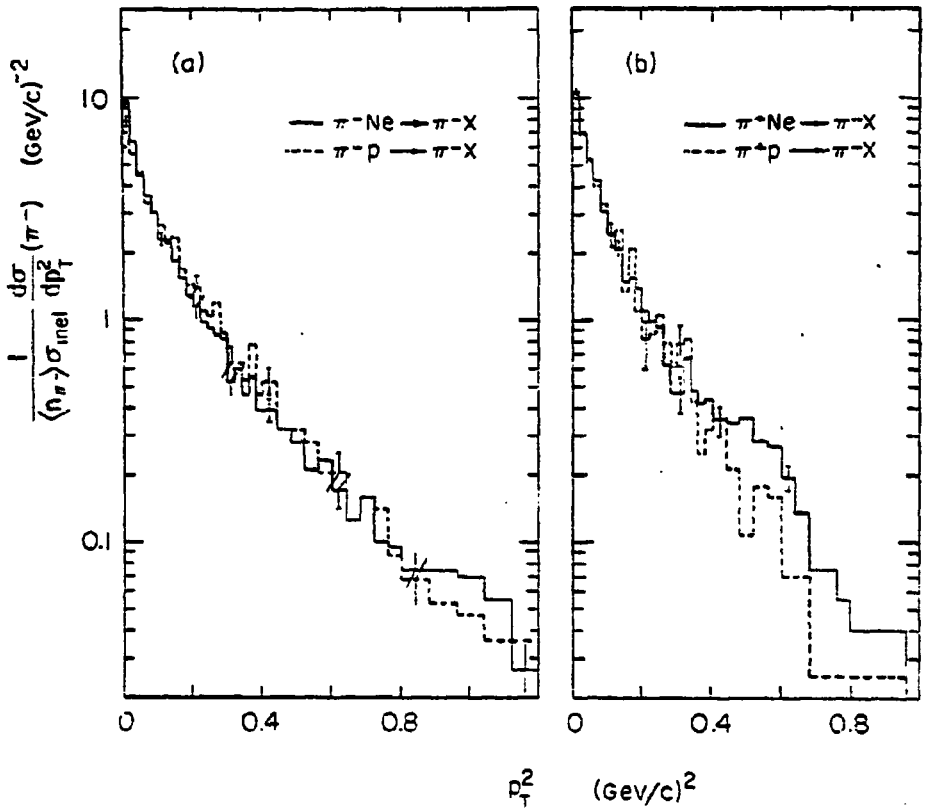
(a)
(b)
π^-Ne → π^-X
π^-p → π^-X
π^+Ne → π^-X
π^+p → π^-X
$\frac{1}{\langle n_\pi \rangle \sigma_{inel}} \frac{d\sigma}{dp_T^2}(\pi^-)$ (Gev/c)$^{-2}$
10
1
0.1
0
0.4
0.8
p_T^2 (Gev/c)^2

Fig. 12.

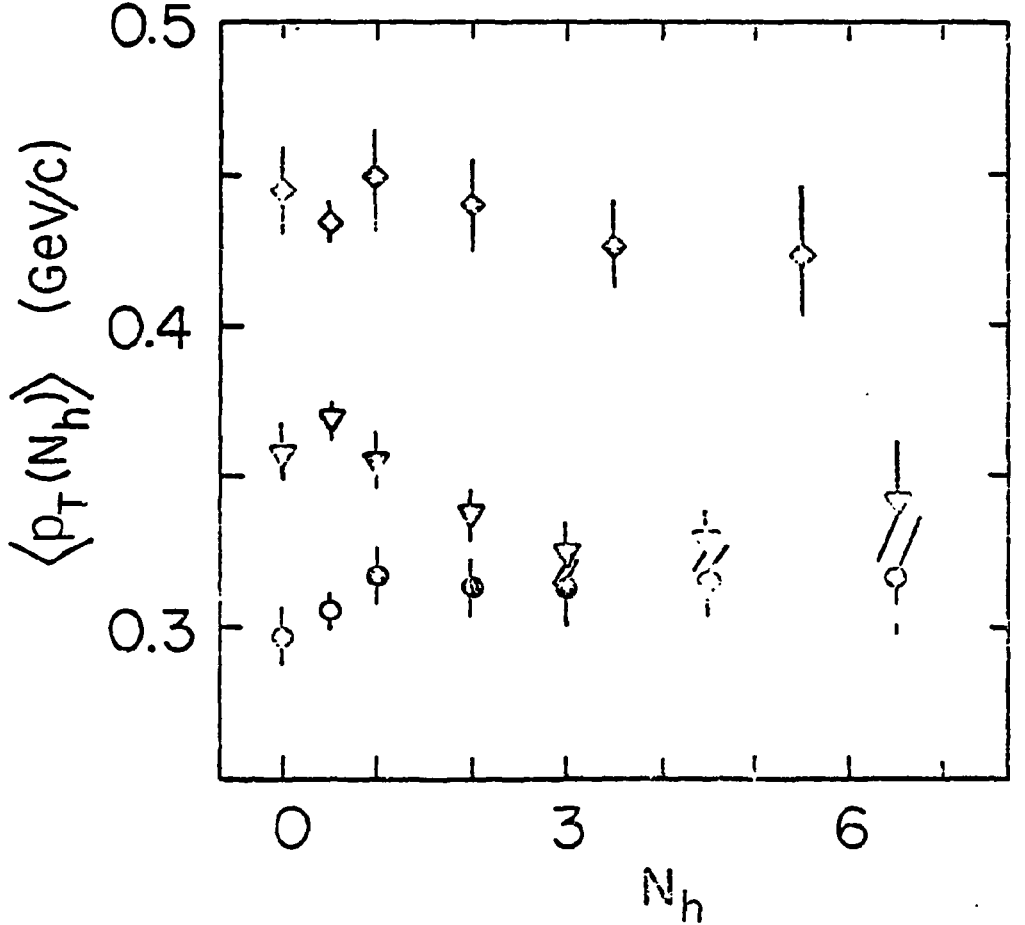
0.5
0.4
0.3
$\langle p_T(N_h) \rangle$ (GeV/c)
0
3
6
N_h

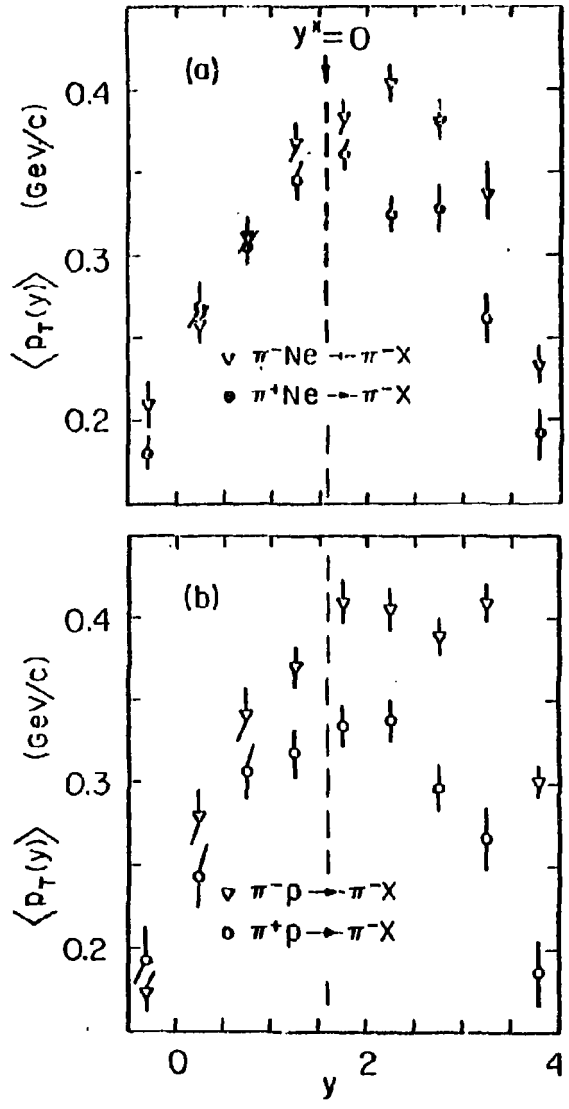
y*=0
(a)
0.4
0.3
0.2
(GeV/c)
⟨pT(y)⟩
▽ π⁻Ne → π⁻X
● π⁺Ne → π⁻X
(b)
0.4
0.3
0.2
(GeV/c)
⟨pT(y)⟩
▽ π⁻p → π⁻X
○ π⁺p → π⁻X
0
2
4
y

Fig. 14.

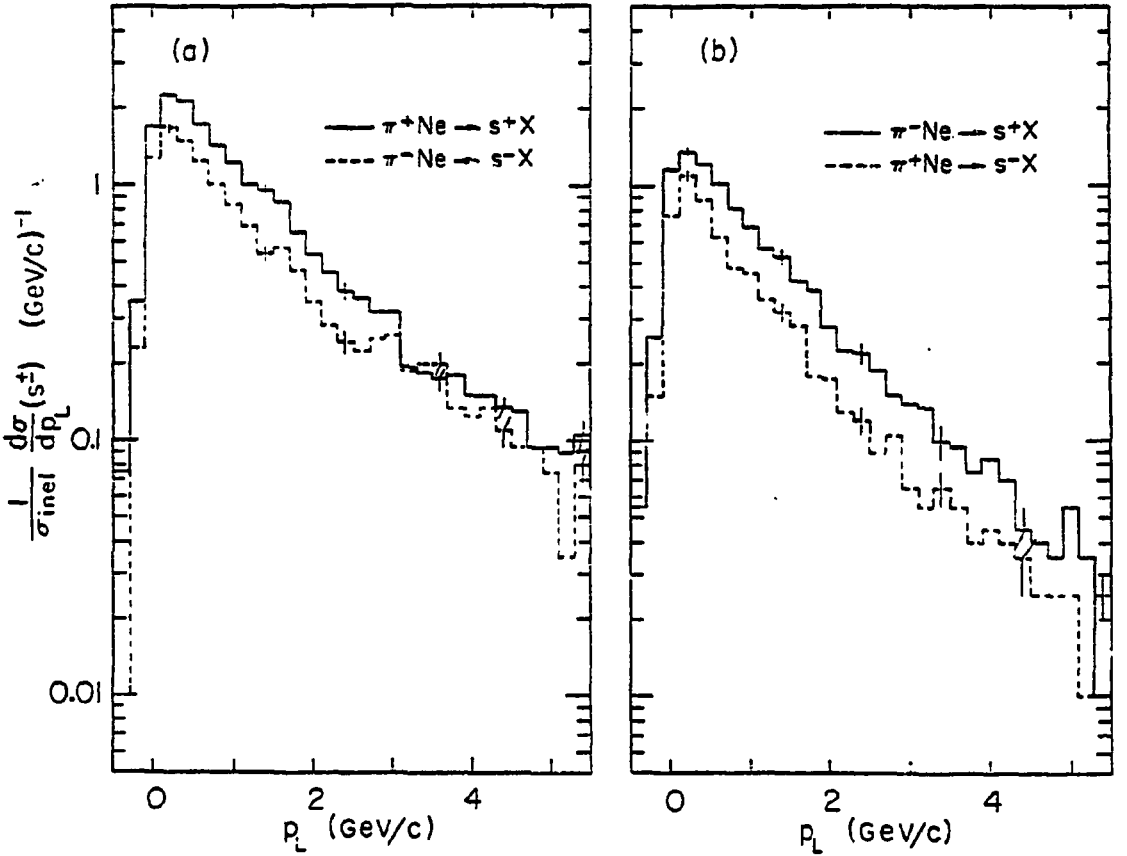
(a)
(b)
$\pi^+Ne \rightarrow s^+X$
$\pi^-Ne \rightarrow s^-X$
$\pi^-Ne \rightarrow s^+X$
$\pi^+Ne \rightarrow s^-X$
$\frac{1}{\sigma_{inel}} \frac{d\sigma}{dp_L}(s^\pm)$ (GeV/c)$^{-1}$
1
0.1
0.01
0
2
4
p_L (GeV/c)

Fig. 15

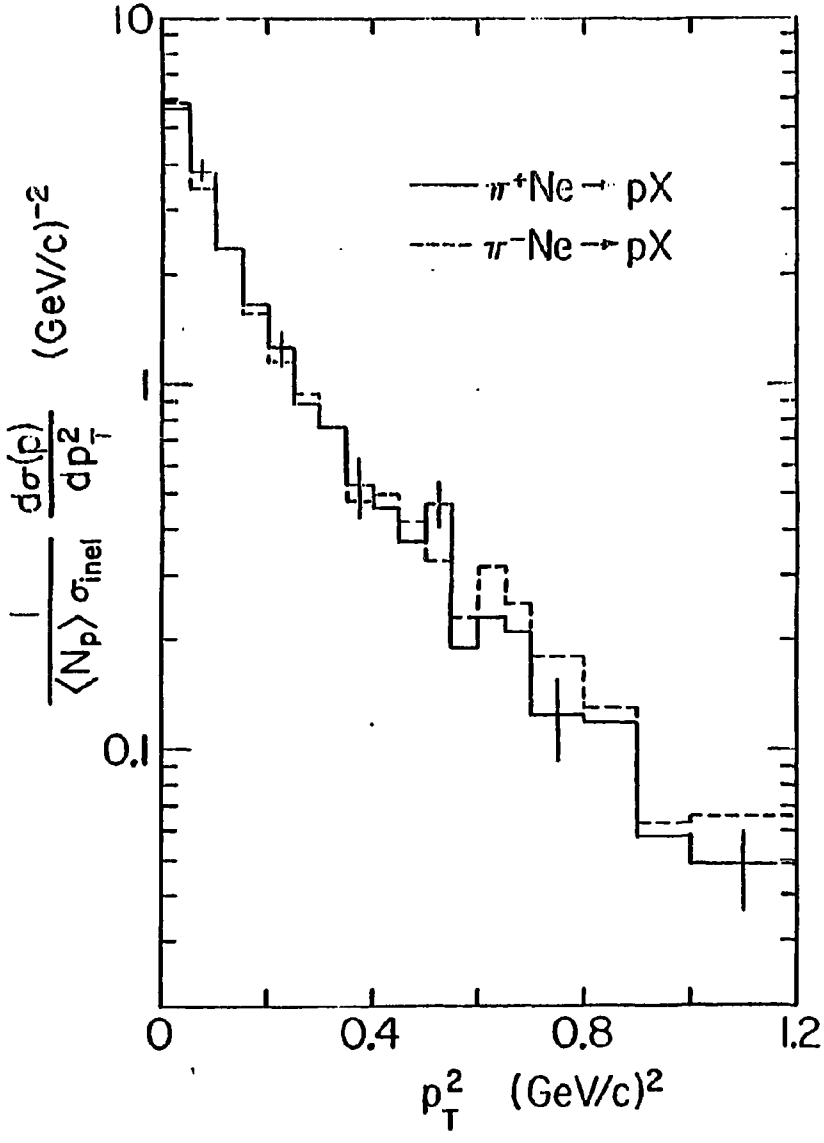
10
1
0.1
0
0.4
0.8
1.2
$\pi^+ Ne \rightarrow pX$
$\pi^- Ne \rightarrow pX$
$\frac{1}{\langle N_p \rangle \sigma_{inel}} \frac{d\sigma(p)}{dp_T^2}$ (GeV/c)$^{-2}$
p_T^2 (GeV/c)^2

Fig. 16

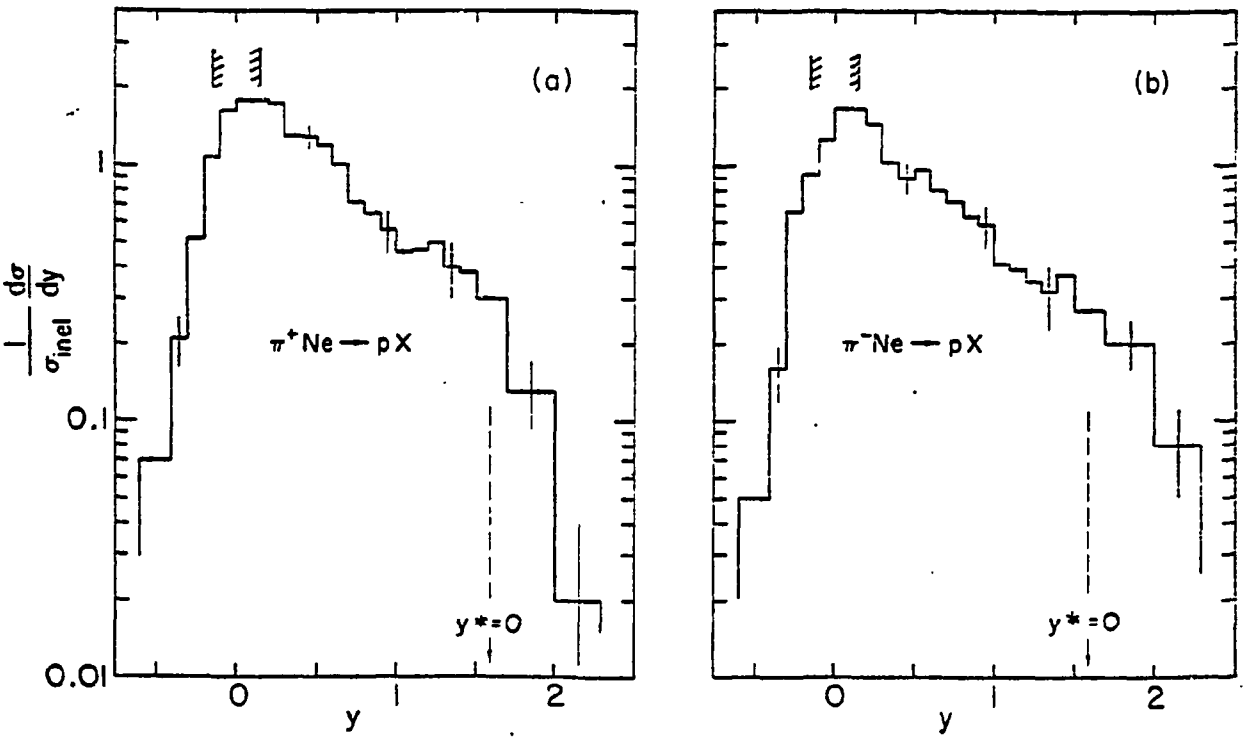
(a)
(b)
$\frac{1}{\sigma_{inel}}\frac{d\sigma}{dy}$
1
0.1
0.01
$\pi^+ Ne \rightarrow pX$
$\pi^- Ne \rightarrow pX$
y* = 0
y* = 0
0
1
2
0
1
2
y
y

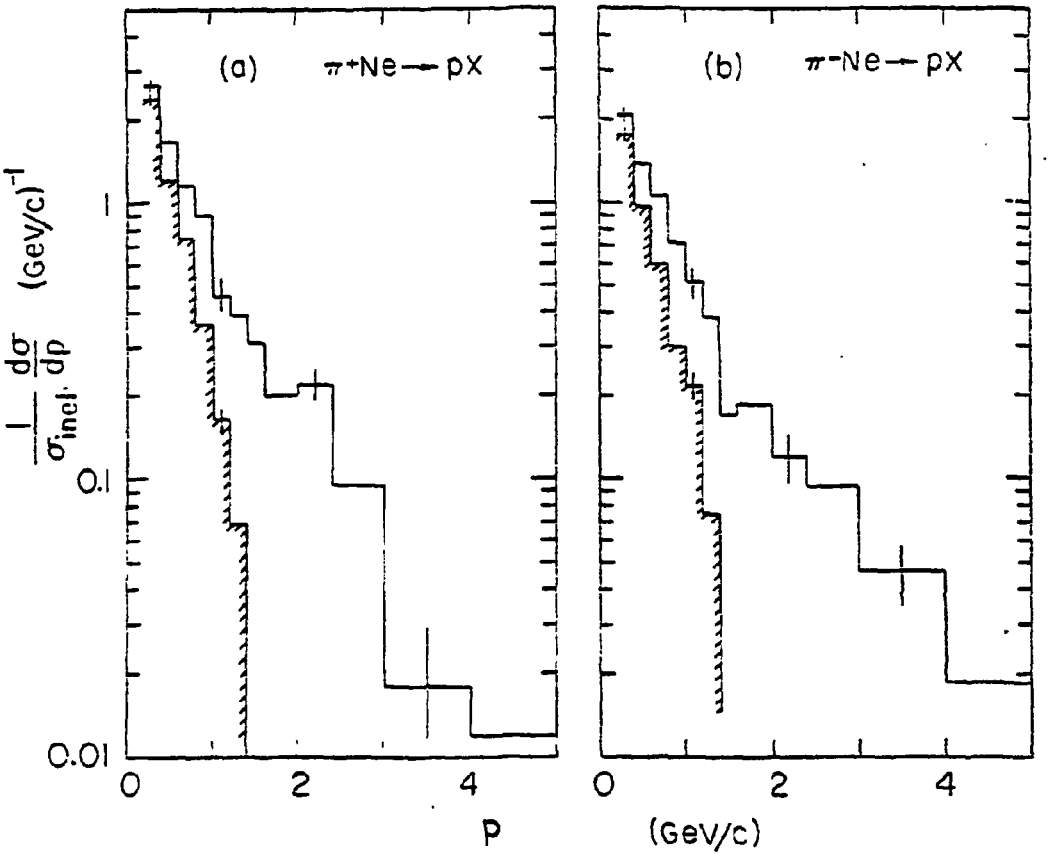
(a) π⁺Ne → pX
(b) π⁻Ne → pX
$\frac{1}{\sigma_{inel}} \frac{d\sigma}{dp}$ (GeV/c)⁻¹
0.1
0.01
0
2
4
p
(GeV/c)

Fig. 18.

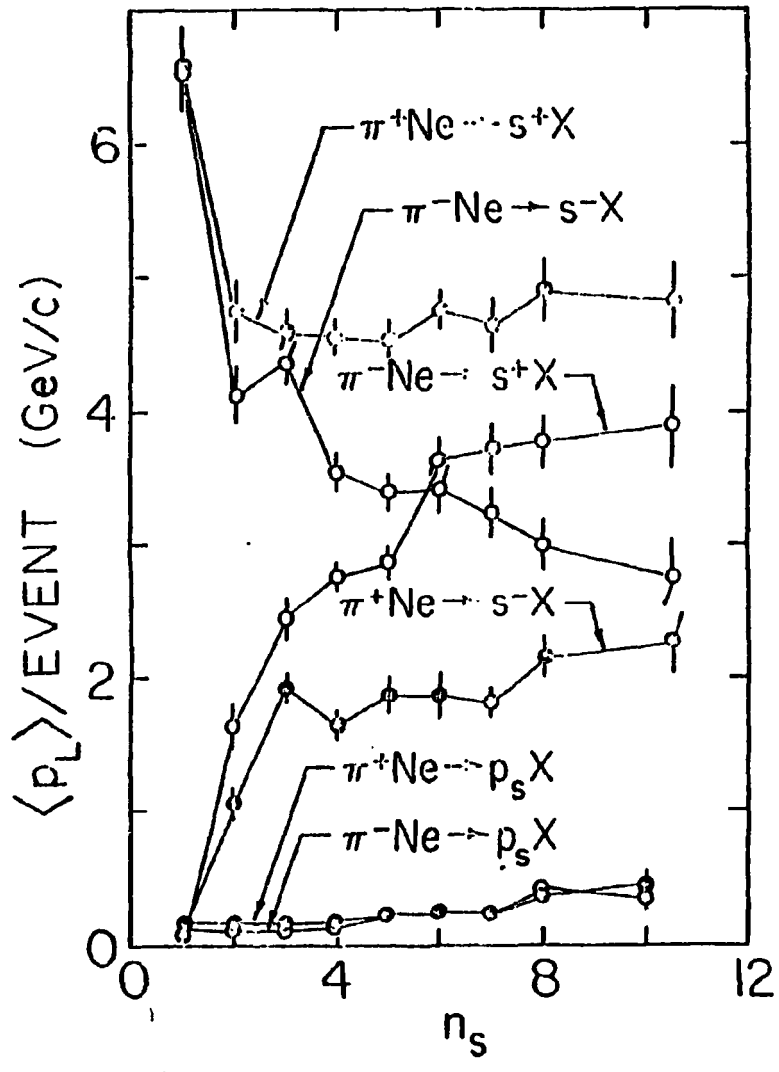
$\pi^+Ne \rightarrow s^+X$
$\pi^-Ne \rightarrow s^-X$
$\pi^-Ne \rightarrow s^+X$
$\pi^+Ne \rightarrow s^-X$
$\pi^+Ne \rightarrow p_sX$
$\pi^-Ne \rightarrow p_sX$
$\langle p_L \rangle$/EVENT (GeV/c)
n_s
0
2
4
6
0
4
8
12

Fig. 19.

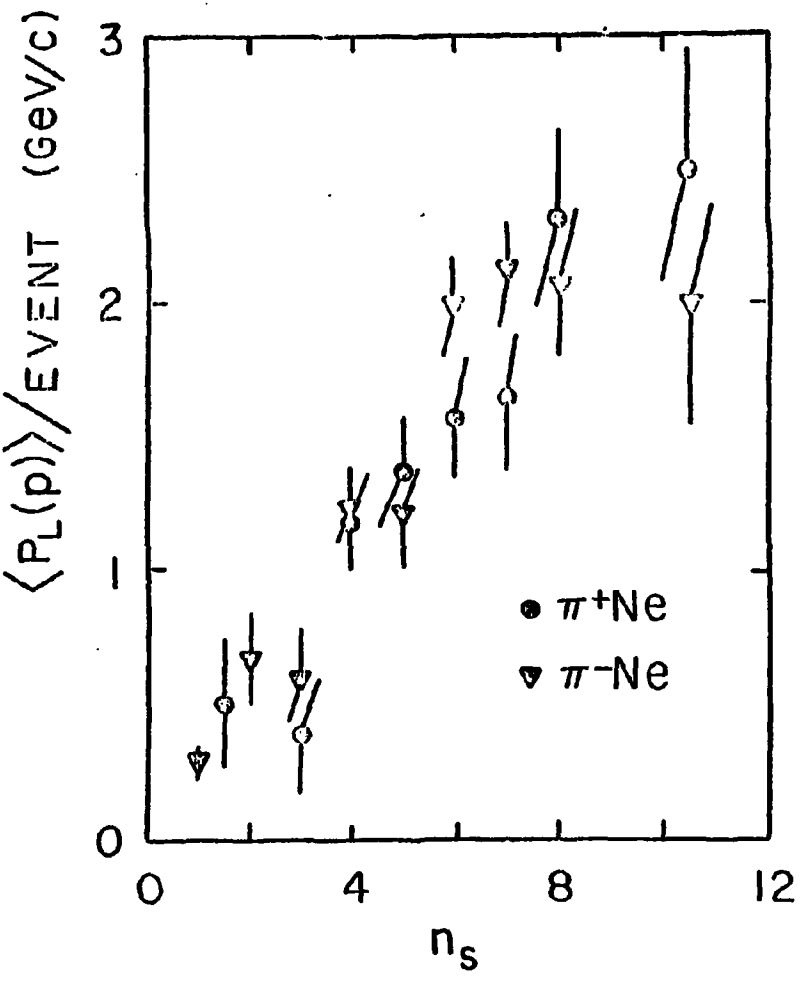

Fig. 20

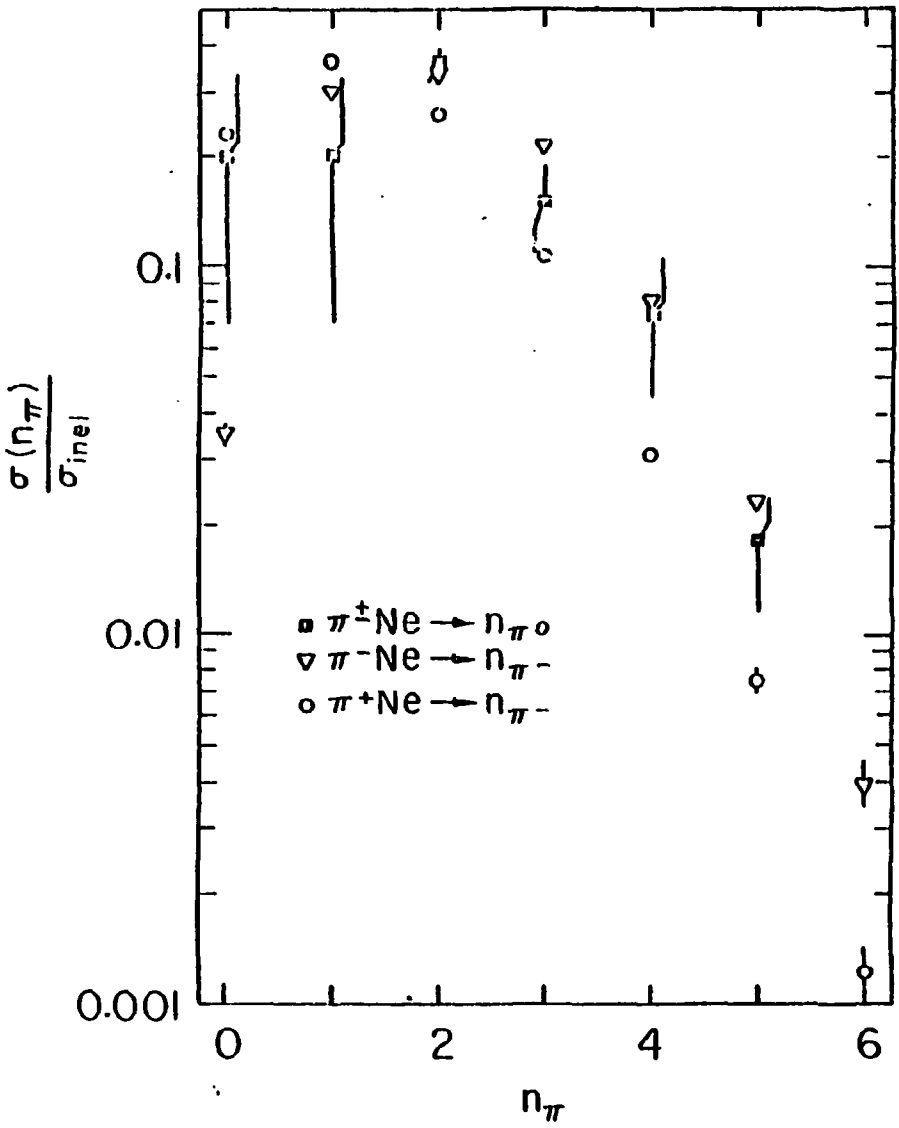
$\frac{\sigma(n_\pi)}{\sigma_{inel}}$
0.1
0.01
0.001
0
2
4
6
n_π
$\pi^{\pm}Ne \rightarrow n_\pi o$
$\pi^{-}Ne \rightarrow n_\pi -$
$\pi^{+}Ne \rightarrow n_\pi -$

Fig. 21

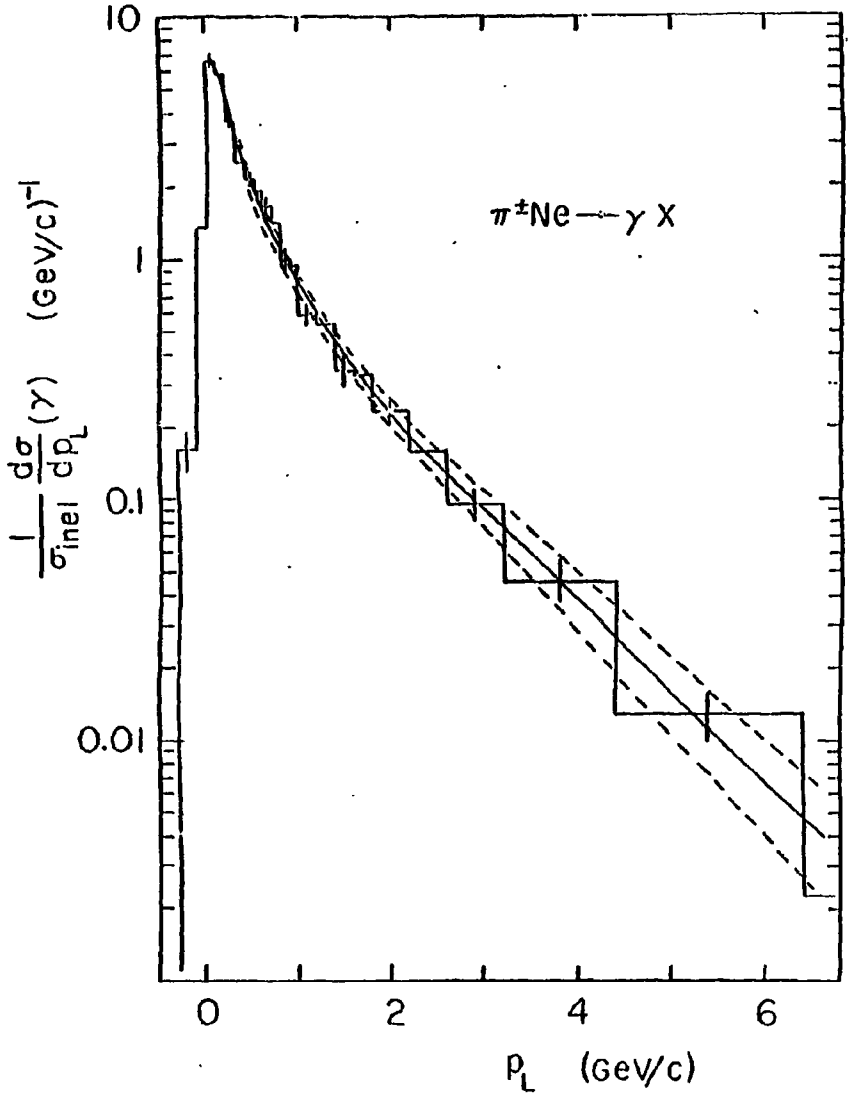
10
1
0.1
0.01
0
2
4
6
$\pi^{\pm}Ne \rightarrow \gamma X$
$\frac{1}{\sigma_{inel}} \frac{d\sigma}{dp_L}(\gamma)$ (GeV/c)$^{-1}$
p_L (GeV/c)

Fig. 22

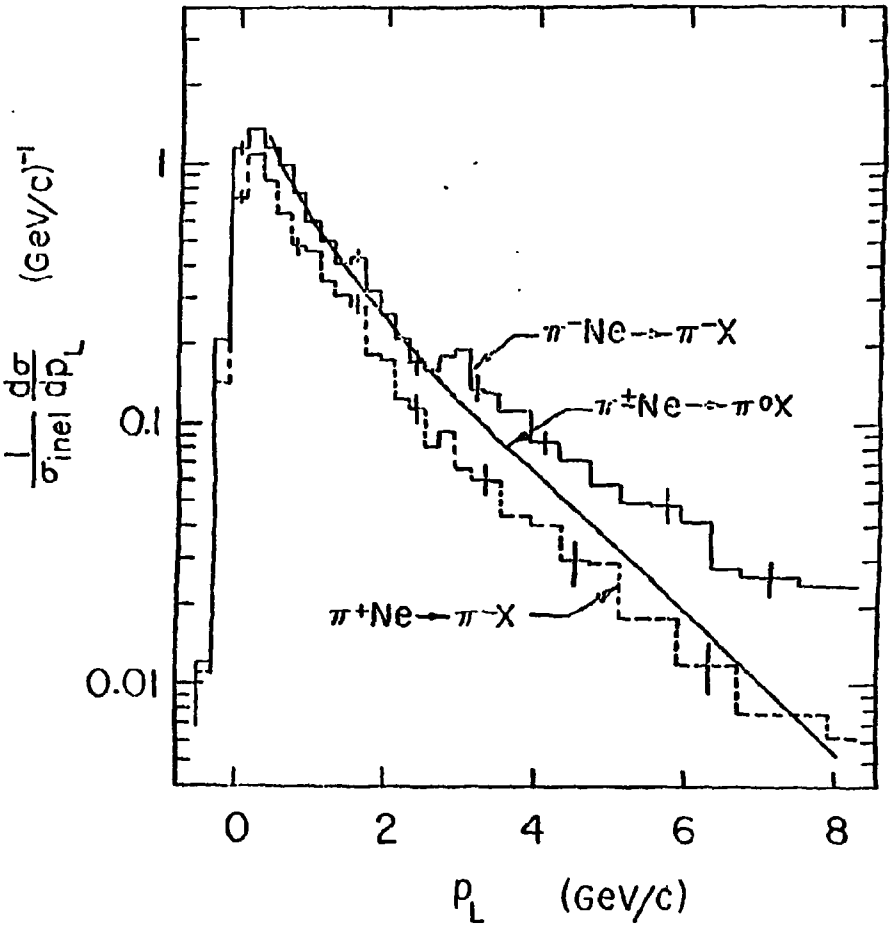
$\frac{1}{\sigma_{inel}} \frac{d\sigma}{dp_L}$ (GeV/c)$^{-1}$
1
0.1
0.01
π^-Ne → π^-X
$\pi^\pm$Ne → π^0X
π^+Ne → π^-X
0
2
4
6
8
p_L (GeV/c)

Fig. 23

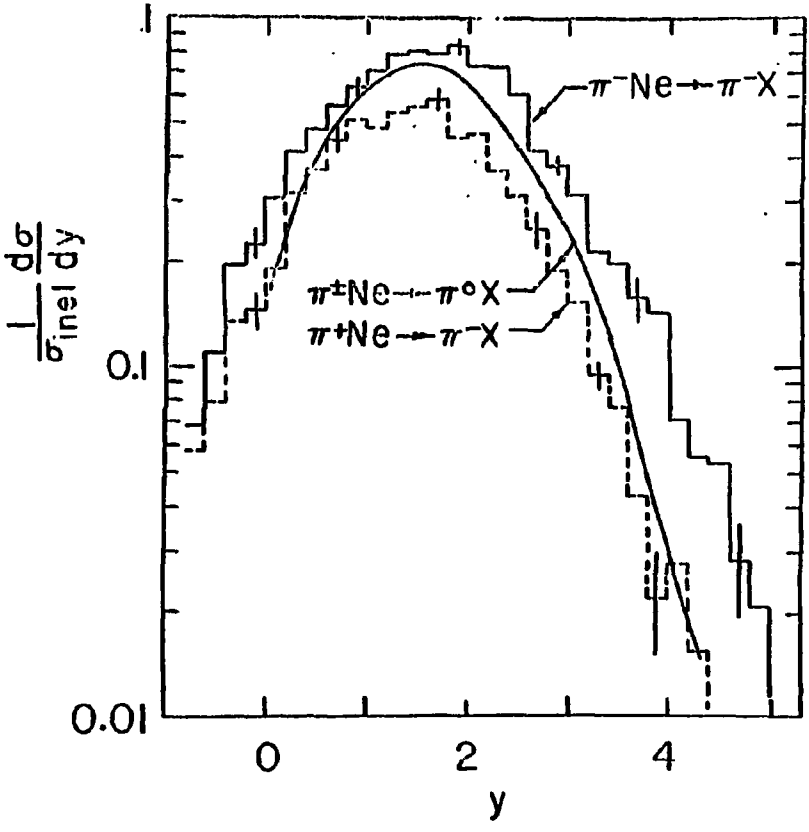
1
0.1
0.01
0
2
4
y
$\frac{1}{\sigma_{inel}}\frac{d\sigma}{dy}$
$\pi^-Ne \to \pi^-X$
$\pi^\pm Ne \to \pi^\circ X$
$\pi^+Ne \to \pi^-X$

Fig. 24